# MØLLER POLARIMETRY WITH ATOMIC HYDROGEN TARGETS

## Project Description

Revision 2
First version: February 22, 2003
Last revision: January, 2005

E.A. Chudakov
Thomas Jefferson National Accelerator Facility

V.G. Luppov
University of Michigan Spin Physics Center

January 20, 2005

**Abstract**

This document describes a novel proposal of using polarized atomic hydrogen gas, stored in an ultra-cold magnetic trap, as the target for electron beam polarimetry based on Møller scattering. Such a target of practically 100% polarized electrons could provide a superb systematic accuracy of about 0.5% for beam polarization measurements. The physics of ultra-cold atomic hydrogen in the magnetic traps is briefly outlined, the main characteristics are optimized to the task of using the stored hydrogen as the target for polarimetry. Although such traps have been built for particle physics applications, the storage cell has not been used so far as the target in a high power beam. Possible impacts the CEBAF beam can make on such a target are discussed, including heating by ionization losses and the impact of the beam electromagnetic (RF) radiation. The conclusion is, although the beam would change slightly the gas properties, as temperature and density, no large depolarization effects should happen, or they can be easily avoided, and the achievable luminosity should be sufficient for beam polarimetry. Finally, such a device has a potential for being used as a target of polarized protons, since the proton polarization gradually and spontaneously increases in the stored hydrogen, up to $\sim 80\%$.
The project was first proposed in 2002 and reported on two conferences [1].

# Contents

# Chapter 1

# Introduction

Of two electromagnetic processes widely used for electron beam polarimetry, the Møller scattering seems to have an advantage over the Compton scattering. Its counting rate does not depend on the energy, the analyzing power is high (about 80%) and neither depends on the energy, nor is changing considerably in the range of the polarimeter acceptance, and two electrons with high energies in the final state make it easy to detect their coincidence and reduce the background no negligible values. Nevertheless, Compton polarimetry is considered more accurate.

Møller polarimeters utilize magnetized ferromagnetic foils as the polarized electron target [2,3,4,5,6,7,8]. Such targets provide electron polarization of about 8%, known typically with an accuracy of about 2-3% relative. There are also other systematic errors associated with the ferromagnetic targets. These targets are heated up by the beam, and, since heating affects the foil polarization, the beam current must be limited to 2-3 $\mu$A. In contrast, the physics experiments often require a much higher current up to 100 $\mu$A. Therefore, the polarization measurements can not run simultaneously with the experiment and have to use a different beam regime, which may be a source of systematic errors, difficult to evaluate.

Another source of the errors are heavy atoms used for the target. Møller scattering off electrons from the internal atomic shells has a distorted energy-angle correlation of the secondary electrons, with respect to scattering off electrons from the external shells. A difference of the polarimeter acceptance to these two classes of events is the source of a systematic error (so-called Levchuk effect [9]), typically of about 1%. This effect forbids using a strong optical collimation of the secondary particles, favorable otherwise for background suppression. In most cases, the background is dominated by electron-nucleus scattering and contains one electron in the final state. It can be efficiently suppressed by detecting both secondary Møller electrons in coincidence. However, for most of the existing Møller polarimeters, this leads to a dead time of about several percent, providing a systematic error hardly much better than 1%. Although, it is possible to reduce considerably the systematic error of the foil polarization by using a very high magnetization field [8], it is difficult to reduce the other errors, in particular the one associated with the beam current limitations.

With all this in mind it seems very attractive to use atomic hydrogen gas, held in an

ultra-cold magnetic trap [10], with 100% polarized electrons, since it would remove all the accuracy limitations discussed above. Here, a feasibility study of such an option is presented. The main questions addressed are:

- Target construction and parameters;
- Target density and polarimeter statistical accuracy;
- The beam influence on the target parameters;
- Possible interference of the target with the beamline and polarimeter operations at Jefferson Lab.

# Chapter 2

# Polarized Atomic Hydrogen Target

## 2.1 General Description

The magnetic field $B_S$ splits the ground states of hydrogen into four states with different energies, their properties are summarized in Tab.2.1 and the energy splitting is shown on Fig. 2.1.

| name | wave function | relative energy E | E/k, in K, at $B_S = 8$ T |
|---|---|---|---|
| $\|d\rangle$ | $\|\uparrow\Uparrow\rangle$ | $\mathcal{H} - \mu_+ B_S$ | 5.394 |
| $\|c\rangle$ | $\alpha\|\downarrow\Uparrow\rangle + \beta\|\uparrow\Downarrow\rangle$ | $\mathcal{H}(-1 + 2\sqrt{1 + (\frac{\mu_- B_S}{2\mathcal{H}})^2})$ | 5.366 |
| $\|b\rangle$ | $\|\downarrow\Downarrow\rangle$ | $\mathcal{H} + \mu_+ B_S$ | -5.360 |
| $\|a\rangle$ | $\alpha\|\uparrow\Downarrow\rangle - \beta\|\downarrow\Uparrow\rangle$ | $\mathcal{H}(-1 - 2\sqrt{1 + (\frac{\mu_- B_S}{2\mathcal{H}})^2})$ | -5.400 |

Table 2.1: Levels of hydrogen in a magnetic field directed along $z$. The symbol $|\downarrow\Uparrow\rangle$ denotes the state with $m_Z = -1/2$ for the electron and $m_Z = +1/2$ for the proton. The constant $\mathcal{H} = 5.87 \cdot 10^{-6}$ eV defines the hyperfine splitting, namely $4\mathcal{H}/h = 1.420$ GHz, while $\mu_+ = \mu_e + \mu_p$ and $\mu_- = \mu_e - \mu_p$ ($\mu_e < 0$.) The factors $\alpha$ and $\beta$ can be presented as $\alpha = sin\ \theta$, $\beta = cos\ \theta$, where the mixing angle $tan\ 2\theta \approx 0.05/B_S(T)$. At $B_S$ =8 T the admixture of the "wrong" polarization is $\alpha \approx 0.3\%$ in the amplitude and $\sim 10^{-5}$ in the sample.

In a magnetic field gradient a force $-\nabla(\vec{\mu_H}\vec{B})$ pulls two lower energy states into the stronger field and repels the higher two states outside. The 0.3 K cylindrical storage cell is located in the bore of a superconducting ∼8 T solenoid. The polarized hydrogen is confined along the cell axis by the magnetic field gradients, and by the wall of the cell laterally (Fig. 2.2).

At the point of statistic equilibrium the state population follows the Boltzmann distribution:

$$n \propto \exp(\mu_e B/kT) \tag{2.1}$$

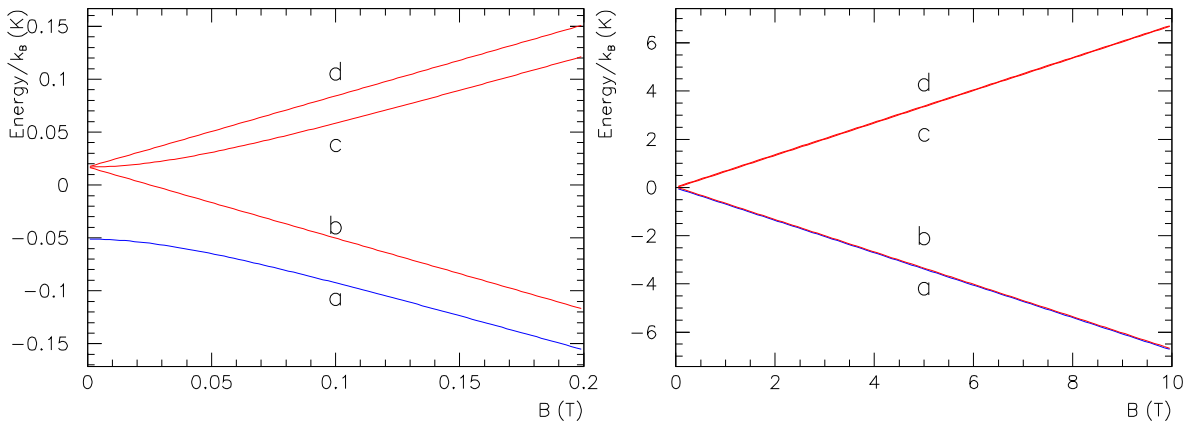


Figure 2.1: Splitting of hydrogen levels in magnetic fields (for low and high fields).

The cell is mainly populated with the states $|a\rangle$ and $|b\rangle$, with an admixture of the states $|c\rangle$ and $|d\rangle$ of $\exp(-2\mu_e B/kT) \approx 3 \cdot 10^{-16}$. In the absence of other processes, the states $|a\rangle$ and $|b\rangle$ are populated nearly equally. Since the state $|a\rangle$ has a $|\uparrow\downarrow\rangle$ component (see Tab.2.1), the electron polarization of the gas would be $\sim (1 - 10^{-5})$.

The hydrogen density is limited mainly by the process of its recombination into $H_2$ molecules (releasing ∼4.5 eV). This process is stronger at lower temperatures. In gas, recombination in collisions of two atoms is kinematically forbidden and is allowed in collisions of three atoms. On the walls, there is no kinematic limitation. At moderate gas densities only the surface recombination matters. In case of polarized atoms, the cross section of recombination is strongly suppressed, because two hydrogen atoms in the triplet electron spin state have no bound states. This fact leads to the possibility of reaching relatively high gas densities in the traps for polarized atoms.

A way to reduce the surface recombination on the walls of the storage cell is coating them with a thin film (∼50 nm) of superfluid $^4$He. The trap itself is usually made of pure copper. The helium film has a very low sticking coefficient for hydrogen atoms. In contrast, hydrogen molecules in thermal equilibrium with the film are absorbed and frozen in clusters on the metal surface of the trap [11].

The higher energy states leave the storage cell, or recombine within it into hydrogen molecules which eventually are either frozen on the helium coated wall, or leave the cell by diffusion. Outside of the helium covered cell the atoms promptly recombine on surfaces and the molecules are either pumped away or are frozen on the walls.

The cell is filled with atomic hydrogen from an RF dissociator. Hydrogen passes through a Teflon pipe to a nozzle, entering at ∼30 K a system of helium coated baffles, where it is cooled down to ∼0.3 K. At 30 K no recombination occurs because of the high temperature, while at 0.3 K it is suppressed by helium coating. In the input flow, the atoms and molecules are mixed in comparable amounts, but most of the molecules are frozen out in the baffles and do not enter the cell.

The gas arrives to the area of a strong field gradient which separates at this moment

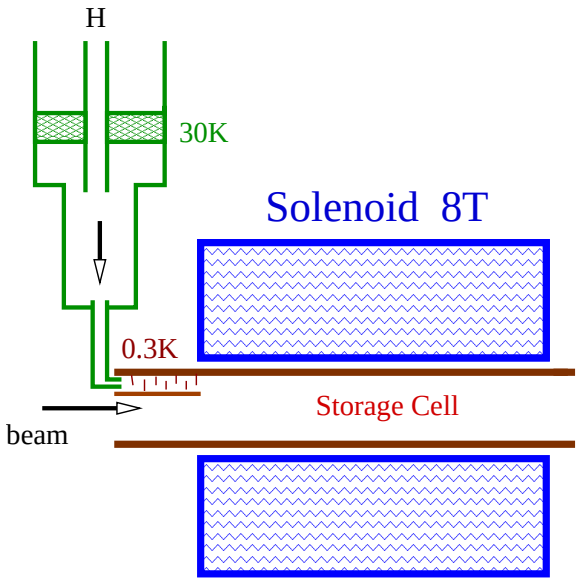


Figure 2.2: A sketch of the storage cell

the lower and higher atomic energy states, therefore a constant feeding of the cell does not affect the average electron polarization.

This technique was first successfully applied in 1980 [12], and later a density[1] as high as $3 \cdot 10^{17}$ atoms/cm$^3$ in a small volume was achieved [10]. It was then proposed to use the high density stabilized ultra-cold electron-spin-polarized atomic hydrogen in proton-spin-polarized sources and targets [13, 14, 15] by means of extraction the gas from the storage cell and creating a jet of polarized atoms. So far, the storage cell itself has not been put in a high intensity particle beam.

For the project discussed a normal storage cell design can be used, with the beam passing along the solenoid axis (Fig. 2.2). The double walls of the copper cell form a dilution refrigerator mixing chamber. The cell is open on both ends toward the beam pipe. The tentative cell parameters are:

- Solenoid length $L_S = 40$ cm;
- Cell internal radius $r_\circ = 2$ cm;
- Cell length $L_C = 45$ cm;
- Maximum field $B_S = 8$ T;
- Temperature $T = 0.3$ K.

The magnetic field distribution $B_Z(Z)$ on the axis of the solenoid is illustrated on Fig. 2.3. The gas density dependence on the coordinate $z$ along the solenoid axis follows

[1] This parameter is called concentration, but we will use the word density in the text, since the mass of the gas is not important here.

Eq. 2.1 and is shown on Fig. 2.3.

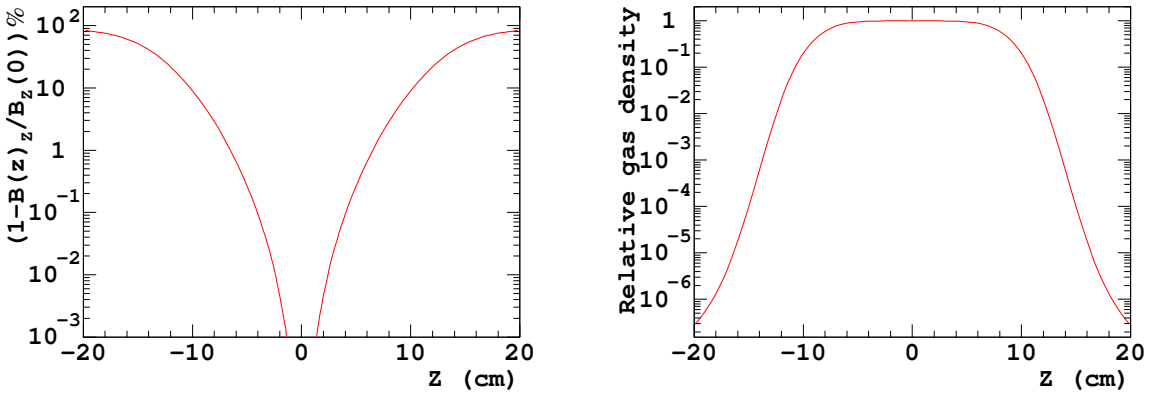


Figure 2.3: Left plot: The relative difference of the longitudinal magnetic field in the solenoid with the field at the solenoid center. Right plot: the gas relative density distribution along the solenoid axis. The field map of a uniform solenoid B8030-5 from AMI [31] was used.

The effective length of such a target is about 20 cm. The solenoid field has to be reasonably uniform in this volume of the cell, in order to avoid areas with the gas density higher than on the axis, since such an area would increase the recombination speed without increasing the luminosity. The field in the volume should not exceed the field at the solenoid center by more than $\sim 2 \cdot 10^{-3}$ (a $\sim$4% increase in the density).

For the guideline, we will consider a gas density of $3 \cdot 10^{15}$ cm$^{-3}$, obtained experimentally [16], for a similar design.

## 2.2 Gas Properties

Important parameters of the target gas are the diffusion speed and heat conductance. At 300 mK the speed RMS is:

$$\overline{v} = \sqrt{8kT/\pi m} = 80 \text{ m/s}; \qquad \sqrt{\overline{v_z^2}} = \sqrt{kT/m} = 48 \text{ m/s}. \tag{2.2}$$

The number of collisions per second depends on the atomic scattering cross section $\sigma$ ( [17]):

$$\frac{dn_{col}}{dt} = \sigma \cdot 4n\sqrt{\frac{kT}{\pi m}} = 4d^2 \cdot n\sqrt{\pi\frac{kT}{m}}, \tag{2.3}$$

where $n$ is the gas density, $m$ is the atomic mass and $d = \sqrt{\sigma/\pi}$ is the effective atom diameter. The mean free path $\ell$ and its projection on a certain direction, say $z$, $\ell_z$ are:

$$\ell = \overline{v}/\frac{dn_{col}}{dt} = (\pi d^2 n\sqrt{2})^{-1}, \qquad \ell_z = \sqrt{\overline{v_z^2}}/\frac{dn_{col}}{dt} = (4d^2 n\sqrt{\pi})^{-1}. \tag{2.4}$$

There are several calculations of the hydrogen atoms cross sections [18, 19, 20, 21, 22] at low temperatures. One should point out that in the bulk of the polarized hydrogen all the atomic collisions happen in the triplet state of electron spins, while the converted atoms in this gas would interact also in the singlet state. The interaction cross sections in these two states must be different, since the triplet interaction potential is purely repulsive, while the singlet one is partially attractive [23].

| Reference | | conditions | H polarized | | H unpolarized | |
|---|---|---|---|---|---|---|
| No. | Ref., date | | $\sigma$, $10^{-16}$ cm$^2$ | $d$, $10^{-8}$ cm | $\sigma$, $10^{-16}$ cm$^2$ | $d$, $10^{-8}$ cm |
| 1 | [19], 1971 | T>1 K | 87.0 | 5.26 | 68.0 | 4.65 |
| 2 | [20], 1977 | T∼0 K | 42.3 | 3.69 | - | - |
| 3 | [21], 1980 | T∼0 K | 6.5 | 1.44 | 4.9 | 1.25 |
| 4 | [22], 1983 | T=2.5 K | ∼30.0 | 3.10 | - | - |

Table 2.2: Cross sections of atomic interactions in polarized and unpolarized atomic hydrogen gas.

A large spread of the results (see Tab.2.2) requires a further investigation of the subject. For these studies we accepted the value $\sigma = 42.3 \cdot 10^{-16}$ cm$^2$, or $d = 3.69 \cdot 10^{-8}$ cm, ignoring the difference between the triplet and singlet cross sections. This would provide $\frac{dn_{col}}{dt} \approx 1.4 \cdot 10^5$ sec$^{-1}$ and $\ell = 0.57$ mm, $\ell_z = 0.34$ mm at 0.3 K and density of $3 \cdot 10^{15}$ cm$^{-3}$.

The average time for a "low field seeking" atom to travel to the edge of the cell at $|z| = 22.5$ cm was estimated using simulation, taking into account the gas density distribution along Z and the repelling force in the magnetic field gradient. This is the cleaning time for an atom with opposite electron spin, should it emerge in the cell, if it does not recombine before. The cleaning time depends on the position of the atom's origin (see Fig. 2.4, left). The cleaning time depends on the gas parameters as follows:

$$\tau_d \propto \frac{d^2}{\sqrt{T}} n, \qquad \langle \tau_d \rangle \approx 0.7 \text{ s}. \tag{2.5}$$

The average cleaning time is about 0.7 s, while the average collision time with the walls is about 0.5 ms. While its presence in the cell, the atom practically uniformly populates the cell cross section.

This calculation was done for reasonably dense gas, when $\ell \ll r_\circ$. At densities $< 10^{12}$ cm$^{-3}$ the mean free path is $\ell \gg r_\circ$ and, since the collisions of atoms with the helium coated walls are nearly elastic, the mean time to reach the cell edge is:

$$\tau_f \approx L_C/4 \cdot \sqrt{\frac{m}{kT}} \approx 2 \text{ ms}. \tag{2.6}$$

For the following calculations we use an effective value[2]:

$$\tau_E \approx \sqrt{\tau_d^2 + \tau_f^2} \tag{2.7}$$

[2] The gas mean free path at the high density is about 0.01 of the tube diameter. Therefore, at this

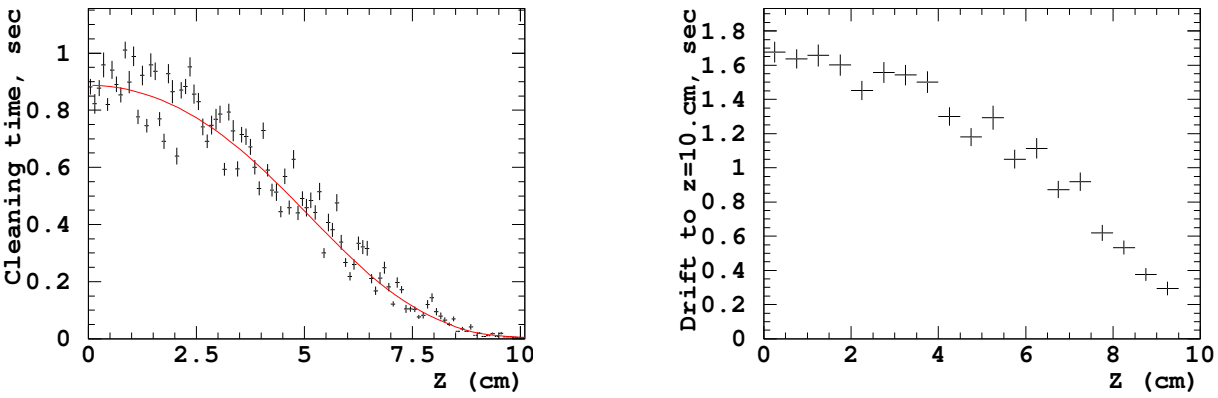


Figure 2.4: Left: Simulated dependence of the cleaning time, or the average time needed for a "low-field-seeking" atom to leave the cell, on the Z-coordinate of the atom's origin. The curve is fit to the simulation and is used for various calculations in this document. Right: Simulated average drift time of a "spinless atom" to the area of a strong field gradient (z=10 cm).

At high enough densities we can define the diffusion factor:

$$D = \frac{2}{3\sigma n}\sqrt{\frac{kT}{\pi m}} \tag{2.8}$$

and the heat conductance (for a monoatomic gas):

$$\chi = \frac{4k}{3\sigma}\sqrt{\frac{kT}{\pi m}} \tag{2.9}$$

dependent on the atomic cross section $\sigma$ and not dependent on the gas density.

## 2.3 Gas Lifetime in the Cell

For the moment we consider the gas behavior with no beam passing through it. Several processes lead to loss of hydrogen atoms from the cell:

1) thermal escape through the magnetic field gradient;

2) recombination in the volume of gas;

3) recombination on the surface of the cell.

The thermal escape 1) can be estimated by calculation of the number of atoms crossing per second the cell cross section $S_s$ toward the cell edge with a longitudinal speed $v_z$, that

density one may use the "viscose" approximation. At lower densities, like at the edge of the cell, or while filling it, Knudsen or molecular approximations should be used. Since we have to understand the gas behavior at very different densities, we have to provide a bridge between these regimes.

$mv_z^2/2 > \mu B$:

$$\frac{dn_{es}}{dt} = S_c \cdot n \cdot \sqrt{\frac{kT}{2\pi m}} \cdot \exp\left(-\mu_e B/kT\right) = \mathcal{E}(T) \cdot n. \tag{2.10}$$

The volume recombination can be neglected up to densities of $\sim 10^{17}$ cm$^{-3}$ [10].

The surface recombination cross section can be characterized by a factor [10]:

$$\mathcal{K}_s^{eff} = 5 \cdot 10^{-8} \frac{A}{V} \Lambda^2 \exp\left(2\varepsilon_a/kT\right) \frac{\sqrt{T}}{B^2}, \tag{2.11}$$

where $A$ is the storage surface area, $V$ is the storage volume, $\Lambda = \hbar\sqrt{\frac{2\pi}{kTm}} \approx 1.74 \cdot 10^{-7}/\sqrt{T}$ is thermal de Broglie wavelength and $\varepsilon \approx 1$ K is the H absorption energy on the He surface. The sizes are measured in cm.

One should note that Eq. 2.11 presents a simplified model, ignoring the difference between states $|a\rangle$ and $|b\rangle$. In reality, a small admixture of the opposite electron polarization in the state $|a\rangle$ considerably increases its recombination rate with both $|a\rangle$ and $|b\rangle$ atoms. Therefore, as a result, the state $|a\rangle$ is depleted faster than $|b\rangle$. If no relaxation between $|a\rangle$ and $|b\rangle$ happens (it may happen on magnetic impurities on the cell surface), the population ratio $|a\rangle/|b\rangle$ drops with time and the recombination rate slows down.

The losses have to be compensated by constant feeding the cell with atomic hydrogen. at a rate of $\Phi \sim 1 - 10 \cdot 10^{15}$ atoms/s. The balance condition is:

$$\frac{\Phi}{V} = \mathcal{K}_s^{eff}(T) \cdot n^2 + \frac{\mathcal{E}(T)}{V} \cdot n, \tag{2.12}$$

where $n$ is the gas density. Solutions for this equation for different feed rates, temperatures and magnetic fields are presented on Fig. 2.5. It should be pointed out that the temperature should not exceed ~0.4 K, because of a high helium gas pressure beyond this.

The plots on Fig. 2.5 help to specify the optimal cell parameters:

$$B_S > 7 \text{ T}, \qquad T \sim 0.3 \text{ K}. \tag{2.13}$$

For the $B_S = 8$ T, $T = 0.3$ K and $\Phi = 1 \cdot 10^{15}$ s$^{-1}$ the calculated density is $n \approx 1 \cdot 10^{16}$ cm$^{-3}$, not far from the reference value of $3 \cdot 10^{15}$ cm$^{-3}$. [3] The gas is mostly lost to recombination. The average lifetime of an atom in the cell is $nV/\Phi \sim 1$ h. Comparing this lifetime with the time to travel between the cell edges of ~2.0 s we see that the gas has time to populate the different field areas accordingly to Eq. 2.1.

For $B_S = 8$ T and $T = 0.3$ K the filling rate of the cell and the decay rate, if feeding stops, are shown on Fig. 2.6. In order to speed up filling a variable feed rate is needed.

## 2.4 Gas Population Dynamics and Proton Polarization

The cell is filled with a practically equal mixture of $|a\rangle$ and $|b\rangle$ states, but their lifetimes in the cell are different. It has been already discussed in Sec. 2.3, that a small admixture

[3] This value was measured at 0.2 K.

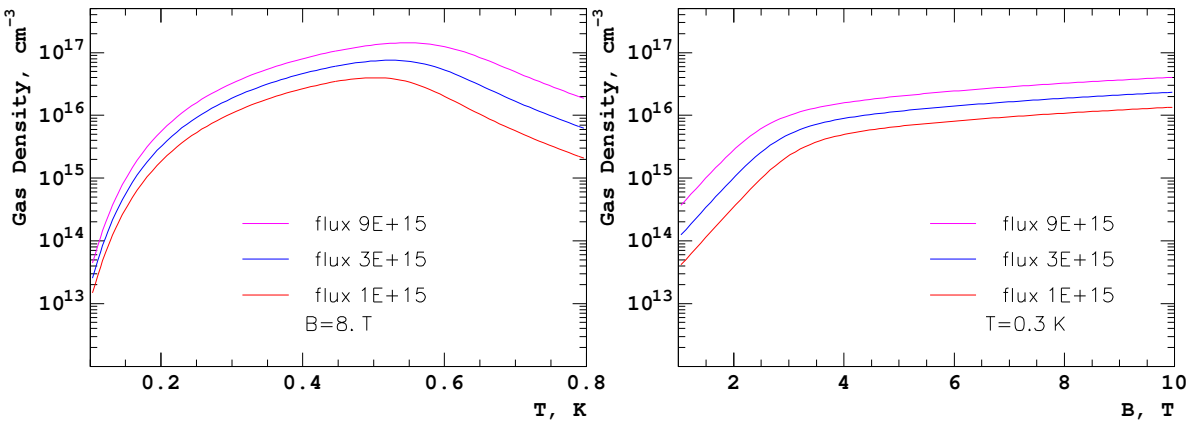


Figure 2.5: Dependence of the stable gas density on the temperature (at 8 T) and the magnetic field (at 300 mK) for different incoming fluxes of hydrogen. The incoming flux has to balance the losses due to surface recombination and the thermal escape through the field gradient. The latter component dominates at $T > 0.55$ K.

of $\uparrow\downarrow$ state in $|a\rangle$ leads to its faster depletion than the state $|b\rangle$. Therefore, after a certain time, while the density in the cell has decreased, the cell will contain predominantly the state $|b\rangle$ atoms, and the protons in the target will become polarized. This effect has been observed [24]. The time scale for proton polarization build-up is about 10 min, and a polarization of $\sim$80% was reached in a dynamic equilibrium. This effect can be destroyed by magnetic impurities in the cell material, which cause $|b\rangle \rightarrow |a\rangle$ mixing.

## 2.5 Unpolarized Contamination

There are several sources of unpolarized contamination in the target gas:

1) hydrogen molecules;

2) high energy atomic states $|c\rangle$ and $|d\rangle$;

3) excited atomic states;

4) other gasses, like helium and the residual gas in the the cell.

The contributions 1)-3) are present when the cell is filled with hydrogen. They are difficult to measure directly, and we have to rely on calculations. We can also estimate their impact indirectly, by making polarization measurements at different conditions, like the density, temperature and beam current. In contrast, the contribution 4) can be easily measured with the beam, taking an empty target measurement. Hydrogen can be completely removed from the cell, by heating a small element inside the cell, which would remove the helium coating on this element, and catalyze a fast recombination of hydrogen on its surface. However, it is important to keep this contamination below several percent in order to reduce the systematic error associated with the background subtraction.

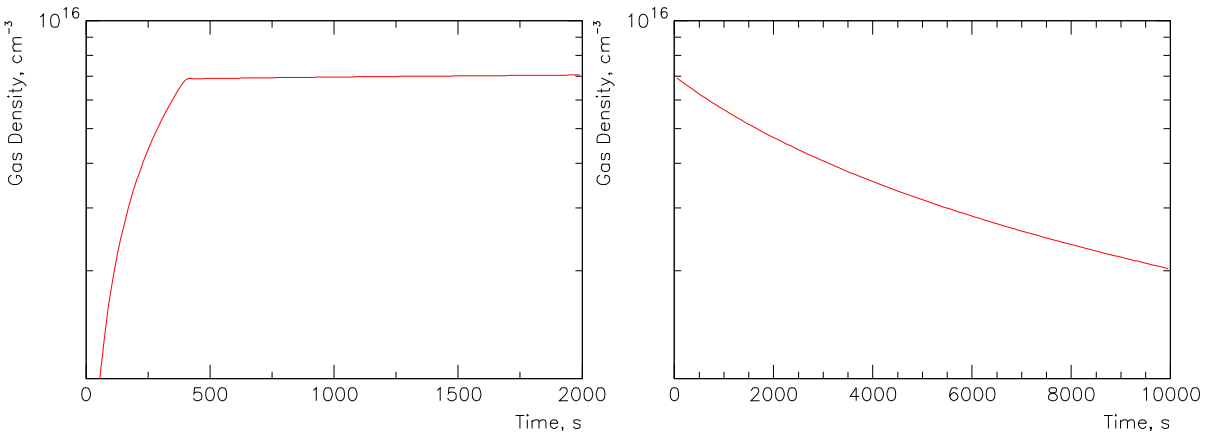


Figure 2.6: Left: density increase while filling the cell. The first $\sim 7$ min the feed rate is $10 \cdot 10^{15}$ atoms/s, after that it is $1 \cdot 10^{15}$ atoms/s. Right: density drop when the feeding gas flow stops. Both curves were calculated for $B_S = 8$ T and $T = 0.3$ K.

For the moment we ignore a possible beam influence.

### 2.5.1 Contamination by Hydrogen Molecules

A hydrogen molecule at 0.3 K travel in the atomic gas in the same way as the atoms. The average diffusion time of Eq. 2.5 should be corrected by a factor $\sqrt{3}$ due to the double mass of the molecule, and by the ratio of the cross sections for molecular-atomic and atomic collisions. For the latter we take the molecular-molecular collision cross section ( [20], Tab.II) with $d = 2.9 \cdot 10^{-8}$ cm. The full correction factor is $\sqrt{3}\frac{2.9^2}{3.7^2} \approx 1$ and therefore the average diffusion is about the same as for atoms. In contrast with atoms, the molecules are absorbed on helium coated surfaces. The atom's rate of collisions with the walls is about 2000 s$^{-1}$. Therefore, one may expect the lifetime of a molecule in gas as $\tau_M \sim 1$ ms.

The residual pressure of hydrogen in the vacuum chamber is less than $10^{-5}$ Torr, contributing less than $10^{-7}$ to the contamination in the cell. The flux of molecules coming with the input flow is less than $10^{14}$ s$^{-1}$, contributing less than $10^{-7}$ to the cell volume.

A source of molecules is the recombination process, discussed in Sec. 2.3. The molecules are produced on the cell surface, then escape into the volume. They have a high speed and are in an highly excited states, since the recombination energy is about 4.5 eV. The molecules kinetic energy can thermally stabilize in about 100 atomic collisions in less that 1 ms. It is considered that for full thermal stabilization about 100 collisions on the walls is needed, which would take $< 50$ ms. Measurements [11] showed a time of about $\tau_M \sim 20$ ms.

The relative contamination on unpolarized atoms is:

$$\eta = \frac{\mathcal{K}_s^{eff} n^2 \cdot \tau_M}{n} = \mathcal{K}_s^{eff} \tau_M n \approx \frac{\tau_M \Phi}{Vn} \approx 6 \cdot 10^{-6} \qquad \text{for } n = 7 \cdot 10^{15} \text{ cm}^{-3} \tag{2.14}$$

The contamination is proportional to the gas density. For the densities under consideration

the contamination is negligible.

In conclusion, the molecular contamination should be below $10^{-5}$ and can be neglected.

### 2.5.2 Contamination by $|c\rangle$ and $|d\rangle$ States

In an ideal case of thermal equilibrium the contribution of the states $|c\rangle$ and $|d\rangle$ is $\sim 10^{-16}$. The lifetime of such an atom in the cell is in fact shorter than the cleaning time (see Eq. 2.5), since they have a high probabitlity to recombine with the $|a\rangle$ and $|b\rangle$ states, which populate the cell. After recombination they produce molecules which do not contribute much to the contamination, because of the short life time in the cell (Sec. 2.5.1). For this analysis, we will use for the $|c\rangle$ and $|d\rangle$ same lifetime as the cleaning time (Eq. 2.5), $\tau_d = 0.7$ s.

Transitions like $|b\rangle \rightarrow |c\rangle$ are suppressed in comparison with the opposite transition, by the Boltzmann factor of Eq. 2.1. The rate has been both calculated and measured $g^{bc} \sim 10^{-15}$ cm$^3$s$^{-1}$ [28] and the contamination is:

$$\frac{\tau_d}{n_b}\frac{dn_c}{dt} \approx g^{bc} \exp\left(-2\mu_e B/kT\right) n_b \cdot \tau_d \sim 10^{-15}, \tag{2.15}$$

where $n_b$ and $n_c$ denote the densities of the states. The effect is negligible.

Some atoms may be excited by collisions with the fast hydrogen molecules. It takes about 100 collisions for a molecule to get thermalized. In this case, the Boltzmann factor does not suppress the transition rate. About $n_m = 10^{15}$ molecules are produced in the cell per second. Each is thermalized in about 0.001 s, since the collision rate is about $10^5$ s$^{-1}$. The total rate of $|c\rangle$ production is $g^{bc} n_b n_m \cdot \tau_d \cdot 10^{-3} \approx 3 \cdot 10^{12}$ s$^{-1}$, or $3 \cdot 10^{-6}$ of the atoms in the cell. The average contamination is $\sim 4 \cdot 10^{-6}$, which is low enough.

### 2.5.3 Contamination by Excited Atomic States

A large energy for ~10 eV is needed to excite the atom in 1S state to the nearest 2S state. Thermodynamically it is forbidden at 0.3 K. For an upper limit, let us suppose that there is a source of such excitations at a level of the recombination rate of $10^{15}$ s$^{-1}$ per cell, or $2 \cdot 10^{12}$ s$^{-1}$cm$^{-3}$, calculated in Sec. 2.3. The lifetimes of excited states with $L > 0$ are typically $\sim 10^{-9}$ s, reducing the contamination to a $\sim 10^{-11}$ level. The excited S states live longer and the state 2S is metastable. However, the S states are subjected to selection of Eq. 2.1, similar to the 1S state. The results of Sec. 2.5.2 apply, and the density of atoms with opposite electron spin should be negligible.

### 2.5.4 Helium and Residual Gas

This contamination does not depend on presence of hydrogen in the cell and therefore can be directly measured with the beam and properly subtracted. However, in order to reduce the systematic errors, the background should not exceed several percent.

The superfluid helium vapor pressure depends strongly on temperature, rising by a factor of $10^3$ between 0.3 K and 0.4 K [25]. A special technique, called "film burners" [25],

is used to prevent the superfluid helium to flow to the warmer parts and evaporate there. At 0.3 K the gas density is about $2 \cdot 10^{12}$ cm$^{-3}$ of electrons, measured in the functioning storage cell with the film burners running[4]. Since the acceptance of the polarimeter is limited to an area less that 30 cm along the beam, the effective target length for helium and hydrogen are comparable and the background from helium should be about $\sim 6 \cdot 10^{-4}$ for the cell density of $\sim 3 \cdot 10^{15}$ cm$^{-3}$.

At JLab, the accelerator residual gas pressure at room temperature is about $1 \cdot 10^{-5}$ Torr. It mainly consists of $N_2$ and water. The corresponding electron density is $3 \cdot 10^{12}$ electrons $\cdot$cm$^{-3}$, or about 0.1% of the electron density of the atomic hydrogen.

The estimated backgrounds are low enough to provide their accurate measurement and subtraction.

[4] A typical pressure $8 \cdot 10^{-7}$ Torr was measured at a room temperature of about 300 K, at a distance from the cryogenic cell, which corresponds to a density of $3 \cdot 10^{10}$ atoms$\cdot$cm$^{-3}$. From this measurement one can derive the density in the cryogenic cell at 0.3 K as $n_{0.3K} = n_{300K} \cdot \sqrt{300K/0.3K} = 10^{12}$ atoms$\cdot$cm$^{-3}$, using the Knudsen rule [29].

# Chapter 3

# Beam Impact on Storage Cell

Let us now discuss possible implications of sending a high intensity electron beam through the storage cell, on the properties of the cell. We consider the following effects:

1) gas heating by the ionization losses (Sec. 3.1);
2) gas excitation and depolarization by the ionization losses (Sec. 3.2);
3) gas depolarization by the RF electromagnetic radiation of the beam (Sec. 3.3);
4) heat load on the cell (Sec. 3.4).

The calculations were done for the CEBAF beam structure (see Sec. A.1.1), but could be applied to other continuous beam accelerators.

## 3.1 Gas Heating by Beam Ionization Losses

In gaseous hydrogen a beam particle releases on average 6.3 MeV/(g/cm$^2$) by ionization. In the target considered, of the thickness $\sim 6 \cdot 10^{16}$ atoms/cm$^2$, the average loss is 0.6 eV per one beam particle. A part of this energy goes to $\delta$-electrons which may leave the cell spiraling in the magnetic field if their energy is large enough. A reasonable cut-off for the $\delta$-electron kinetic energy is $T_1 \sim 1$ keV. At this energy the electron would lose about 100 eV in the target due to ionization losses and carry away the rest of its energy. For the maximum energy we selected $T_2 \sim 0.2 T_{max} = 0.2 E_{beam}$. Then, the full energy carried away by $\delta$-electrons knocked out by one beam particle would be [26]:

$$E = 0.15 \text{ MeV/(g/cm}^2) \cdot \ln \frac{T_2}{T_1} \approx 1.8 \text{ MeV/(g/cm}^2) \tag{3.1}$$

The energy absorbed in the target is $\alpha = 4.5$ MeV/(g/cm$^2$) from one beam particle. The full energy absorbed per unit length of the target per second is:

$$J = \alpha \cdot \frac{\mathcal{I}_b}{q_e} \frac{n}{N_A}, \tag{3.2}$$

where $N_A$ is the Avogadro number and $n$ is the gas density.

The heat conductance in gas is given in Eq. 2.9. Let us assume that the beam profile is flat within a radius $r_b$, which is an approximation in case the beam is not smeared off by a fast raster and is a good model in the presence of a fast raster. Then, solving the heat flow equation for a very long tube, assuming the fixed temperature $T_0$ on the tube wall at $r_\circ$ we obtain:

$$\Delta T(r) = T(r) - T_0 = \frac{J}{2\pi\chi} \ln \frac{r_\circ}{r} \qquad r > r_b$$

$$\Delta T(r) = T(r) - T_0 = \frac{J}{2\pi\chi} \left[ \ln \frac{r_\circ}{r_b} + \frac{1}{2}(1 - \frac{r^2}{r_b^2}) \right] \qquad r < r_b \tag{3.3}$$

The temperature increase reaches the maximum at the beam center:

$$\Delta T(r) = \alpha \cdot \frac{\mathcal{I}_b}{q_e} \frac{n}{N_A} \frac{3\sigma}{8k\pi\sqrt{\frac{kT}{\pi m}}} \left[ \ln \frac{r_\circ}{r_b} + \frac{1}{2} \right] \tag{3.4}$$

and is proportional to the gas density. For $\mathcal{I}_b = 100$ $\mu$A, $n = 3 \cdot 10^{15}$ cm$^{-3}$, $\sigma = \pi d^2$, where $d = 3.7 \cdot 10^{-8}$ cm [20] (see also Tab. 2.2), and $T = 0.3$ K we get:

$$\Delta T(0) = 0.030\ K \cdot \left[ \ln \frac{r_\circ}{r_b} + \frac{1}{2} \right] \tag{3.5}$$

With no convection flow in the gas, the gas density in the absence of external forces follows the Knudsen rule [29]:

$$n \cdot \sqrt{T} = \text{const} \tag{3.6}$$

With the external force of $\mu_e \frac{dB}{dz}$ the density, normalized to one at the initial temperature $T_\circ$ is:

$$n(z) = n_\circ \sqrt{\frac{T_\circ}{T}} \cdot \exp\left( \int_0^z d\xi \frac{dB}{d\xi} \frac{\mu_e}{kT(\xi)} \right). \tag{3.7}$$

At the center of the solenoid $\frac{dB}{dz} \approx 0$ and the density is well described by Eq. 3.6. At the center, the density drops by about 10% and Eq. 3.5 looks like:

$$\Delta T(0) = 0.027\ K \cdot \left[ \ln \frac{r_\circ}{r_b} + \frac{1}{2} \right] \tag{3.8}$$

Very similar results were obtained by solving the appropriate kinetic equations numerically. It was shown also that the temperature practically stays flat along $z$ up to the area of lower density.

With no raster ($r_b \approx 200$ $\mu$m) $\Delta T(0) = 0.14$ K. A raster of $r_b = 2$ mm would decrease it by a factor of $\sim$2: $\Delta T(0) = 0.075$ K.

No serious implication of such a heating is seen. The recombination rate depends only on the temperature on the cell walls, which stays at 0.3 K. The mean polarization should be

not affected in a noticeable way, since the population of oppositely polarized states in the equilibrium would go from $\sim 10^{-16}$ to $\sim 10^{-11}$. The target density change is not important. The average probability to escape through the magnetic gradient would slightly increase, which would move slightly the "filling" curves on Fig. 2.5.

The uncertainty in the gas properties (see Sec. 2.2) may change the results by a factor of two. Even with the double temperature rise no dramatic effect should occur, but one may consider using a fast raster in this case.

The conclusion is that the heating by beam ionization losses should not make a serious impact on the gas storage cell. In order to decide whether a fast raster is needed, a thorough comparison of the theoretical calculations for the transport parameters in the atomic hydrogen has to be done, because of the large difference of the predicted atomic cross sections.

## 3.2 Depolarization by Ionization

Using the estimates from Sec. 3.1 we obtain that a 100 $\mu$A, 0.85 GeV electron beam would loose to ionization and atom excitation $\sim 1.4 \cdot 10^{13}$ eV $\cdot$ s$^{-1}$ per 1 cm of its path. This creates a certain number of free electrons (primary ionization), which may also ionize other atoms (secondary ionization). In hydrogen at normal conditions, it takes on average $\sim$40 eV of the energy loss to create one electron-ion pair. At very low gas density, many of the secondary electrons will escape the volume without ionizing the gas. We use here the value of 40 eV/pair as a lower limit. Then, about $\sim 3.5 \cdot 10^{11}$ pairs $\cdot$ s$^{-1}$cm$^{-1}$ are produced, which means that about $10^{-5}$ of all hydrogen atoms in the cell are ionized per second. The contamination depends on the recombination time and on the spacial distribution of the electrons and ions produced.

Here we face two problems. First, in contrast with neutral atoms, which spread laterally over the cell in $\sim$1 ms because of diffusion, the charged particles would stay in the beam area, moving along the magnetic field lines. Second, the recombination rate of an electron and proton is kinematically forbidden in 2-body collisions, and, in contrast with gas at normal conditions, the 3-body collision rate is very low. The protons will get thermalized in $\sim$1 ms, while electrons in $\sim$10 ms. The charged particles may leave the cell when they reach the magnetic field gradient. Protons and electrons may recombine with atoms into $H_2^+$ and $H^-$ ions, however, again, this recombination is kinematically forbidden in 2-body collisions.

Single protons do not make a background for Møller scattering, but the single electrons and $H_2^+$ or $H^-$ ions may. Assuming the beam area of $4 \cdot 10^{-4}$ cm$^2$ and the cleaning time of the ions and electrons of 0.7 s (the normal diffusion time to the cell edge), we obtain a contamination of $\sim$16%.

A way to remove the charged particles from the beam area is to apply an electric field, perpendicular to the cell axis. The Larmore frequency is $\omega_L = q_e B/m = 1.4 \cdot 10^{12}$ s$^{-1}$ for electrons and $0.8 \cdot 10^9$ s$^{-1}$ for protons. With the typical time between collisions of $\tau = 10^{-5}$ s$^{-1}$ for atoms, $\omega_L \tau \gg 1$ and the charged particles will drift in the crossed fields with

the speed $v = \vec{E} \times \vec{B}/B^2$. With a field of 1 V/cm, at 8 T the speed is 12.5 m/s. Therefore, the lifetime of the charged particles in the beam will be 0.0002 m/12.5 m/s=$1.6 \cdot 10^{-5}$ s, and the potential contamination will be reduced to about $10^{-5}$ level. The positive and negative particles will move to the same direction and eventually recombine on the wall.

There might be a complication in this scheme. The beam creates a radial average electric field. One can calculate it, averaging the field created by one bunch (Eq. A.7) over the repetition time $T$:

$$\overline{E_r(r)} = \frac{q}{2\pi\varepsilon_\circ}\frac{1}{\sqrt{2\pi}\sigma_{Bz}} \cdot (1 - exp(-\frac{r^2}{2\sigma_{Br}^2}))\frac{1}{r}\frac{1}{T}\int_{-T/2}^{T/2} dt \cdot exp(-\frac{t^2}{2\tau_B^2}),$$

and, since $T \gg \tau_B$:

$$\overline{E_r(r)} = \frac{\mathcal{I}_b}{2\pi\varepsilon_\circ c} \cdot (1 - exp(-\frac{r^2}{2\sigma_{Br}^2}))\frac{1}{r} \tag{3.9}$$

also presented on Fig. 3.1. The maximum field of ∼0.2 V/cm is reached at $r \approx 0.2$ mm.

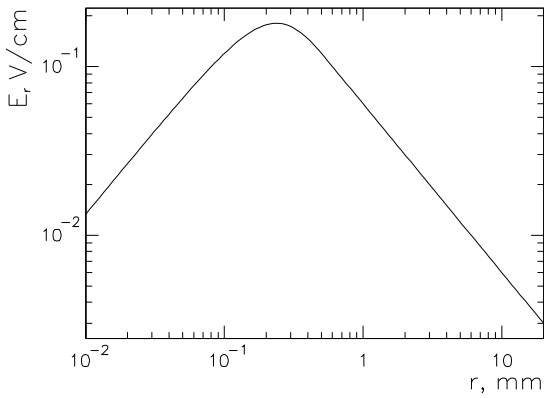


Figure 3.1: Average radial electric field of a 100 $\mu$A beam, depending on the distance from the center. For the transverse beam distribution a Gaussian with $\sigma_{Br} = 0.15$ mm is taken. No rastering is assumed.

This field will not affect the particle motion in a 1 V/cm external field.

The problem of charged particles will be solved, providing a reasonable scheme to mount electrodes inside the storage cell is found. The electrodes should provide a good thermal contact with the cell, while being electrically insulated from it, be covered with the He film and be robust at 0.3 K. Several options are being considered.

## 3.3 Depolarization Caused by the Beam RF radiation

The beam pulses (bunches) produce an electromagnetic wave. This electromagnetic field is calculated in Sec. A.1.2, where all the definitions needed are given.

The magnetic field of the solenoid $B_S$ splits the ground states of hydrogen into four states with different energies, their properties are summarized in Tab.2.1.

The dominant transitions caused by an external electromagnetic wave are those with either electron or proton spin flip. The magnetic field of the wave has to be perpendicular to $z$ to cause a flip, since, say $\langle - |\hat{\sigma}_x| + \rangle = 1$. Indeed, the magnetic field created by the beam is circular and always perpendicular to $z$ (see Eq. A.9). The operator describing the interaction includes both the electron and the proton contributions $\mu_e \hat{\sigma}_x^e + \mu_p \hat{\sigma}_x^p$, but the proton contribution is relatively much smaller and we neglect it. Then, we are left with two transitions, which at $B_S = 8$ T happen at frequencies:

$$|a\rangle \rightarrow |d\rangle \Rightarrow \nu_{ad} = 224.92\ GHz \tag{3.10}$$

$$|b\rangle \rightarrow |c\rangle \Rightarrow \nu_{bc} = 223.50\ GHz \tag{3.11}$$

The probability of a transition, say $|a\rangle \rightarrow |d\rangle$, caused by a harmonic perturbation $\mu_e \cdot B \cdot e^{i\omega t}$, per time unit is:

$$\frac{dV_{a\rightarrow d}}{dt} = \frac{2\pi}{\hbar} \left|\langle d|\mu_e \cdot B \cdot \hat{\sigma}_x^e |a\rangle\right|^2 \delta(\hbar\omega - (E_d - E_a)) \tag{3.12}$$

We neglect the small mixing in the state $|a\rangle$ ($\alpha \rightarrow 0$) and obtain:

$$\frac{dV_{a\rightarrow d}}{dt} = \frac{2\pi}{\hbar^2} \left|\mu_e \cdot B\right|^2 \delta(\omega - \omega_{ad}) \tag{3.13}$$

### 3.3.1 Calculation for the CEBAF beam structure

Let us take into account that the bunches appear at a given frequency, using the Fourier series expansion of Eq. A.18-A.19. Because of non-uniformity of the magnetic field $B_S$ in the volume of the trap there is a considerable spread of $\omega_{ad}$ in the gas sample. We should take into account the appropriate density $\frac{dP}{d\omega_{ad}}$. This density is peaked at the maximum field in the solenoid and has a tail to lower frequencies (see Fig. 3.2). In [25] an RF absorption spectrum for a hydrogen trap at 5 T was presented. The shape of the spectrum is comparable to the simulated one on Fig. 3.2.

The probability of a transition per second can be expressed as:

$$\frac{dV_{a\rightarrow d}}{dt} = \frac{2\pi}{\hbar^2} \sum_{k=-\infty}^{\infty} \left|\mu_e \hat{B}_k(r)\right|^2 \int_{-\infty}^{\infty} d\omega_{ad} \frac{dP}{d\omega_{ad}} \delta(\omega_{ad} - \omega_\circ k). \tag{3.14}$$

Using Eq. A.20 we obtain:

$$\frac{dV_{a\rightarrow d}}{dt} = \sum_{k=-\infty}^{\infty} \left.\frac{dP}{d\omega_{ad}}\right|_{\omega_\circ k} \frac{1}{2\pi} \cdot \left(\frac{\mu_\circ \mu_e \mathcal{I}_b}{\hbar r_\circ}\right)^2 \cdot exp(-\omega_\circ^2 k^2 \tau^2) \cdot G^2(r). \tag{3.15}$$

In order to evaluate the contamination caused by the conversion discussed, we should take into account several features of the trapped gas. First, the cleaning time (the average

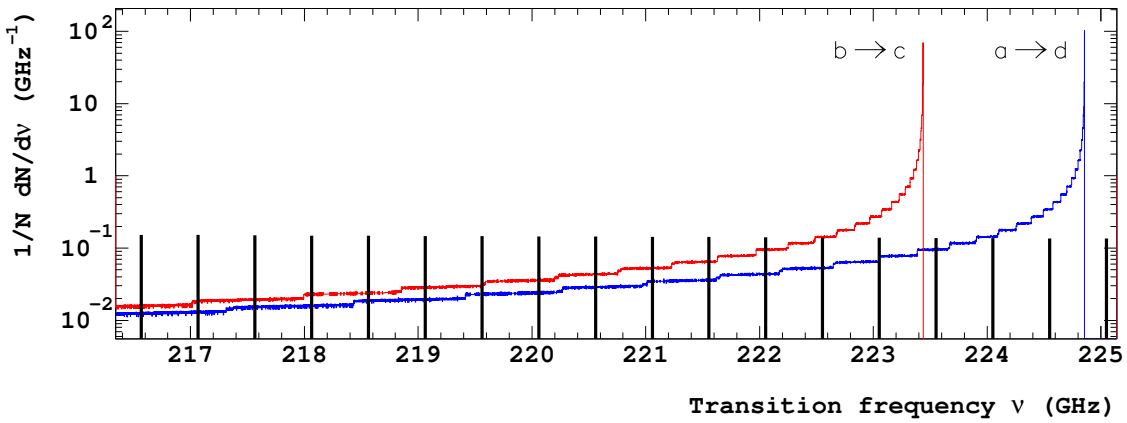


Figure 3.2: Simulated spectra of the transitions on the axis of the hydrogen trap at 7.997 T, for a solenoid B8030-5 from AMI [31]. AMI (American Magnetics, Inc.) provided us with the field distribution of this magnet. The magnet has a $10^{-5}$ uniformity inside the 1 cm diameter central sphere. The density of atoms depends on the field as $exp(-\mu_e B/kT)$. The transitions $|a\rangle \to |d\rangle$ and $|a\rangle \to |c\rangle$, along with the beam frequency grid are shown.

time it takes a "low-field-seeking" atom in $|c\rangle$ or $|d\rangle$ state to leave the cell) depends on the Z-position of the atom's origin (see Fig. 2.4). Second, the cleaning time is ∼1000 times larger than the wall collision time (see Sec. 2.2). Therefore, the atoms in $|c\rangle$ and $|d\rangle$ states, although created by the RF-induced conversion mostly in the beam area, populate the cell cross section practically uniformly before leaving the cell, and we need to calculate only the the average conversion rate over the cell cross section. The full conversion rate inside a cylinder of radius $R$ is:

$$\frac{dV_{a\to d}}{dt}(r<R) = \frac{1}{\pi R^2}\int_0^R dr\cdot 2\pi r\cdot \frac{dV_{a\to d}}{dt} \tag{3.16}$$

Using the approximation from Eq. A.12 we obtain:

$$\frac{dV_{a\to d}}{dt}(r<R) \approx \sum_{k=-\infty}^{\infty} \left.\frac{dP}{d\omega_{ad}}\right|_{\omega_\circ k} \frac{1}{2\pi}\cdot\left(\frac{\mu_\circ\mu_e\mathcal{I}_b}{\hbar}\right)^2\cdot exp(-\omega_\circ^2k^2\tau^2)\cdot\frac{2}{R^2}\cdot(1.205+\ln\frac{R}{5\sigma_{Br}}) \tag{3.17}$$

In order to evaluate the contamination we must take into account the cleaning time $\tau_d$ dependence on the Z-coordinate of the atom (see Fig. 2.4), and, therefore, its dependence on the transition frequency $\omega_{ad} = \omega_\circ k$. Taking the full cell radius $R = r_\circ$:

$$\frac{N_d}{N_a} \approx \frac{1}{\pi}\cdot\left(\frac{\mu_\circ\mu_e\mathcal{I}_b}{\hbar r_\circ}\right)^2\cdot(1.205+\ln\frac{r_\circ}{5\sigma_{Br}})\sum_{k=-\infty}^{\infty}\left.\frac{dP}{d\omega_{ad}}\right|_{\omega_\circ k}\cdot exp(-\omega_\circ^2k^2\tau^2)\mathcal{I}_b\cdot\tau_{dk}, \tag{3.18}$$

where $N_d$ is the concentration of the oppositely polarized $|d\rangle$ state, while $N_a$ is the concentration of the trapped $|a\rangle$ state. The index $k$ in $\tau_{dk}$ indicates that the cleaning time for a

$|d\rangle$-state atom depends on the transition frequency, via its dependence on the location of the $|a\rangle \rightarrow |d\rangle$ conversion point.

The non-uniformity of the magnetic field and the associated non-uniformity of the gas density lead to a strongly peaked gas spectral distribution, which overlaps with a multitude of $\omega_\circ k$ peaks, as shown on Fig. 3.2, obtained by simulation of a trap in the field of a highly uniform solenoid. One should be able, by adjusting the magnetic field, tune the cell in a way that the beam resonances stay beyond the peaks in the gas spectral density, in order to reduce the transitions. It may help to use a solenoid with a more uniform field, in particular more uniform in the area close to the beam. Then, more atoms on the beam path stay beyond the RF grid. Calculating the sum of Eq. 3.18 we add several most contributing terms (see Tab.3.1).

The average contamination calculated for 100 $\mu$A beam is:

$$\frac{N_-}{N_+} \approx 0.0015\% \tag{3.19}$$

The effect depends quadratically on the beam current and is very sensitive to the value of the magnetic field. By tuning the field one can increase the transition rate of either $|a\rangle \rightarrow |d\rangle$ or $|b\rangle \rightarrow |c\rangle$ by a factor of 100. This can be used to study the effect, but would require a possibility to trim the field on a $10^{-4}$ level.

### The Uncertainty of the Calculations

The calculation is sensitive to several parameters which have some degree of uncertainty.

**The beam parameters** mostly are known well enough. The most uncertain parameter is the beam spot size, which depends on the optics of the given beam tune. We used a value of $\sigma_{Br} = 100$ $\mu$m. Since the dependence on this value is logarithmic, in case of $\sigma_{Br} = 30$ $\mu$m (the reasonably minimal radius) the effect grows to $\approx$ 0.0018%.

**The gas parameters** , namely the atomic cross section, is known with a considerable uncertainty (see Table 2.2). The cleaning time is proportional to this cross section. We used the value $\sigma = 42.3 \cdot 10^{-16}$ cm$^2$ [21]. The highest value obtained in another calculation [19] was about twice larger. This would increase the contamination to about $\approx$ 0.003%. The value we used was calculated for polarized gas (atoms collide in spin triplet state only). The calculations [19] and [21] predict a slightly lower cross section in unpolarized gas. In fact, we are interested in collisions of oppositely polarized atoms, therefore we consider the value we used as an upper limit.

**The magnetic field uniformity** affects the spectral density of the gas at the RF resonances. We used the field of an appropriate solenoid. We also calculated the effect for a very simple solenoid of the same size, with a constant current density. The contamination went up to $\approx$ 0.003%.

| k | $\nu = \nu_\circ k$, GHz | Z, cm | $dP/d\omega$, GHz$^{-1}$ | $\tau_{dk}$, sec | contribution to contamination |
|---|---|---|---|---|---|
| transition $\|a\rangle \rightarrow \|d\rangle$ | | | | | |
| 1 | 224.550 | 4.33 | 0.0549 | 0.550 | 0.87E-05 |
| 2 | 224.051 | 5.30 | 0.0225 | 0.401 | 0.26E-05 |
| 3 | 223.552 | 5.85 | 0.0156 | 0.318 | 0.14E-05 |
| 4 | 223.053 | 6.24 | 0.0118 | 0.261 | 0.90E-06 |
| 5 | 222.554 | 6.55 | 0.0082 | 0.220 | 0.53E-06 |
| 6 | 222.055 | 6.80 | 0.0068 | 0.188 | 0.38E-06 |
| 7 | 221.556 | 7.02 | 0.0057 | 0.162 | 0.27E-06 |
| 8 | 221.057 | 7.22 | 0.0055 | 0.141 | 0.23E-06 |
| 9 | 220.558 | 7.39 | 0.0047 | 0.124 | 0.17E-06 |
| 10 | 220.059 | 7.55 | 0.0036 | 0.109 | 0.12E-06 |
| 11 | 219.560 | 7.70 | 0.0038 | 0.097 | 0.11E-06 |
| 12 | 219.061 | 7.83 | 0.0032 | 0.086 | 0.82E-07 |
| 13 | 218.562 | 7.96 | 0.0029 | 0.077 | 0.67E-07 |
| 14 | 218.063 | 8.08 | 0.0025 | 0.069 | 0.51E-07 |
| total | | | | | 0.16E-04 |
| transition $\|b\rangle \rightarrow \|c\rangle$ | | | | | |
| 1 | 223.053 | 4.54 | 0.0419 | 0.518 | 0.63E-05 |
| 2 | 222.554 | 5.40 | 0.0229 | 0.385 | 0.26E-05 |
| 3 | 222.055 | 5.91 | 0.0148 | 0.308 | 0.13E-05 |
| 4 | 221.556 | 6.29 | 0.0103 | 0.254 | 0.77E-06 |
| 5 | 221.057 | 6.59 | 0.0086 | 0.214 | 0.54E-06 |
| 6 | 220.558 | 6.84 | 0.0070 | 0.183 | 0.38E-06 |
| 7 | 220.059 | 7.06 | 0.0057 | 0.158 | 0.27E-06 |
| 8 | 219.560 | 7.25 | 0.0051 | 0.138 | 0.21E-06 |
| 9 | 219.061 | 7.42 | 0.0045 | 0.121 | 0.16E-06 |
| 10 | 218.562 | 7.58 | 0.0038 | 0.107 | 0.12E-06 |
| 11 | 218.063 | 7.72 | 0.0036 | 0.095 | 0.10E-06 |
| 12 | 217.564 | 7.85 | 0.0030 | 0.085 | 0.76E-07 |
| 13 | 217.065 | 7.98 | 0.0029 | 0.076 | 0.65E-07 |
| 14 | 216.566 | 8.09 | 0.0025 | 0.068 | 0.50E-07 |
| total | | | | | 0.13E-04 |

Table 3.1: Calculation of the sum in Eq. 3.18 for AMI solenoid [31] includes adding the results for several resonant frequencies, see Fig. 3.2. Each frequency is associated with a certain Z-coordinate of the atom in the cell. The field at the center of the solenoid was 7.998 T.

**We conclude** that the contamination discussed is below $\approx$ 0.005% within reasonable variations of the input parameters. The effect is proportional to $q^2 \cdot \mathcal{F} = \mathcal{I}_b^2/\mathcal{F}$, where $q$ is the bunch charge. The repetition rate $\mathcal{F}$ defines the density of the resonant frequency lines. The contamination, while negligible at a continuous beam accelerator like CEBAF, can become prohibitively large at a storage ring, unless the bunch length is much longer than at CEBAF (0.5 ps).

### 3.3.2 Calculation for a Randomized Beam

Let us compare the results obtained for a resonant beam structure, with a somewhat simplified case of a "randomized structure", when bunches are arriving at random instead of a fixed frequency (499 MHz at CEBAF). Let us first calculate the probability that a single bunch causes the transition, using the Fourier transform as in Eq. A.17:

$$\hat{B} = B_\circ(r) \cdot \tau \cdot exp(-\frac{\omega^2\tau^2}{2}) \tag{3.20}$$

$$V^B_{a\to d} = \frac{2\pi}{\hbar^2}\int_{-\infty}^{\infty} d\omega \left|\mu_e \cdot \hat{B}\right|^2 \delta(\omega - \omega_{ad}) = 2\pi\left(\frac{\tau\mu_e B_\circ(r)}{\hbar}\right)^2 \cdot exp(-\omega_{ad}^2\tau^2) \tag{3.21}$$

We obtain:

$$V^B_{a\to d} = \left(\frac{\mathcal{I}_b}{\mathcal{F}}\right)^2\left(\frac{\mu_\circ\mu_e}{2\pi\hbar r_\circ}\right)^2 \cdot exp(-\omega_{ad}^2\tau^2)G^2(r) \tag{3.22}$$

At $r = r_\circ = 2$ cm $V^B_{a\to d} = 1.8 \cdot 10^{-14}$, while at the point of the highest field $r = 160$ $\mu$m $V^B_{a\to d} = 1.5 \cdot 10^{-10}$. One bunch does not change the gas polarization in any noticeable way.

If the beam bunches were arriving at random, we could obtain the transition probability per second by multiplying the result of Eq. 3.22 by the repetition rate $\mathcal{F}$:

$$\frac{dV_{a\to d}}{dt} = \frac{\mathcal{I}_b^2}{\mathcal{F}}\left(\frac{\mu_\circ\mu_e}{2\pi\hbar r_\circ}\right)^2 \cdot exp(-\omega_{ad}^2\tau^2)G^2(r) \tag{3.23}$$

which, at $r = 160$ $\mu$m, is $V_{a\to d} = 7.5\%$ s$^{-1}$ and at $r = r_\circ$ is $0.9 \cdot 10^{-5}$ s$^{-1}$. The fraction of the atoms in the cell, converted per second at a given radius is shown on Fig. 3.3 In the same way as for Eq. A.12, for $R > 5\sigma_{Br}$:

$$\begin{aligned}\frac{dV_{a\to d}}{dt}(r<R) &\approx \frac{\mathcal{I}_b^2}{\mathcal{F}}\left(\frac{\mu_\circ\mu_e}{2\pi\hbar r_\circ}\right)^2 \cdot exp(-\omega_{ad}^2\tau^2) \cdot \frac{2r_\circ^2}{R^2} \cdot (1.205 + \ln\frac{R}{5\sigma_{Br}}) \\ &\overset{R=r_\circ}{=} \frac{1}{2\pi^2}\frac{1}{\mathcal{F}}\left(\frac{\mu_\circ\mu_e\mathcal{I}_b}{\hbar r_\circ}\right)^2 \cdot exp(-\omega_{ad}^2\tau^2) \cdot (1.205 + \ln\frac{r_\circ}{5\sigma_{Br}})\end{aligned} \tag{3.24}$$

The conversion rate in a small cylinder $R = 5\sigma_{Br} = 0.5$ mm around the beam is 3.6% $s^{-1}$, while in the full cell of $R = r_\circ = 2$ cm the rate is $0.9 \cdot 10^{-4}$ s$^{-1}$. The average cleanup time is 0.7 s2.5 reduces the contamination to $0.6 \cdot 10^{-4}$ s$^{-1}$. This result is slightly larger than the result3.19 obtained for the realistic beam structure optimized to avoid the resonances.

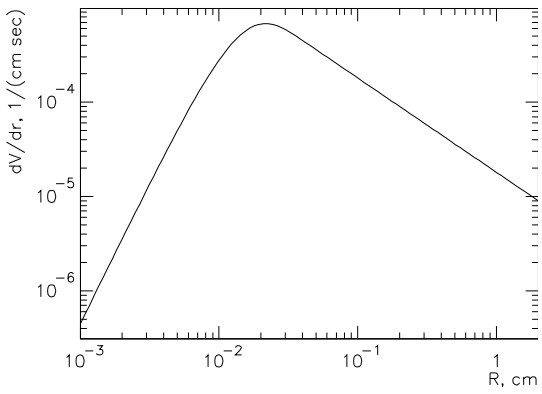


Figure 3.3: The fraction of the atoms in the cell, converted per second at a given radius $\frac{2\pi r}{\pi r_\circ^2}\frac{dV_{a\to d}}{dt}$. Most of the transitions happen at $r \approx 200$ $\mu$m.

### 3.3.3 Depolarization Caused by the RF Radiation of Single Electrons

Single electrons, passing by an atom, create strong fields. Let us consider a possible depolarization from single electrons, in the same way as was done in Sec. 3.3.2 for a bunch, but using the field created by the electron and integrating the effect down to the atom radius.

The electron electric field in its CM frame is boosted to the lab frame in the same way as in Sec. A.1.2:

$$B_T(r,t) = \frac{q_e\gamma}{4\pi\varepsilon_\circ c}\frac{1}{r^2}\cdot\frac{1}{\left(1+(\gamma ct/r)^2\right)^{3/2}}. \tag{3.25}$$

The Fourier transform is:

$$\widehat{B}_T(r,\omega) = \frac{q_e\gamma}{4\pi\varepsilon_\circ c}\frac{1}{r^2}\cdot\frac{1}{\sqrt{2\pi}}\int d\omega e^{-i\omega t}\frac{1}{\left(1+(\gamma ct/r)^2\right)^{3/2}}. \tag{3.26}$$

Let us evaluate this function for $\omega_{ad} \sim 2\pi\cdot 220$ GHz·rad. The useful range of $t$ is $t < 10r/(\gamma c) < 3\cdot 10^{-14}$ s. At this value of $t$ the exponential is close to 1, since $\omega_{ad}t \approx 0.04$. Therefore:

$$\widehat{B}_T(r,\omega_{ad}) \approx \frac{q_e\gamma}{4\pi\varepsilon_\circ c}\frac{1}{r^2}\cdot\frac{1}{\sqrt{2\pi}}\frac{2r}{c\gamma} = \frac{q_e\mu_\circ}{2\pi\sqrt{2\pi}}\frac{1}{r} \tag{3.27}$$

In the same way as Eq. 3.23:

$$\frac{dV_{a\to d}}{dt} = \frac{\mathcal{I}_b}{q_e}2\pi\left(\frac{q_e\mu_\circ\mu_e}{2\pi\sqrt{2\pi}\hbar r}\right)^2 \tag{3.28}$$

Integrating over the radius, assuming a dependence as $1/r_a^2$ for $r < r_a$ ($r_a \sim 10^{-8}$ cm is the atom radius) and $1/r^2$ for $r > r_a$, with a cell radius of $r_\circ$:

$$\frac{dV_{a\to d}}{dt} = \frac{\mathcal{I}_b}{q_e}2\pi\left(\frac{q_e\mu_\circ\mu_e}{2\pi\sqrt{2\pi}\hbar}\right)^2\pi\cdot\left(1+2\ln\frac{r_\circ}{r_a}\right) \sim 10^{-12}\ \mathrm{s}^{-1}. \tag{3.29}$$

The transition probability is negligible.

## 3.4 Cell Heating

Due to calculations in Sec. A.1.2 the total RF radiation coming with the beam has a power of ∼2 mW at 100 $\mu$A. It is argued in Sec. A.1.5 that copper at 0.3 K is nearly purely reflective to the electromagnetic waves and that the energy loss by the 100 $\mu$A beam from the eddy currents or wave absorption should not exceed $\sim$ 3 $\mu$W. This can be compared with ∼1 mW of power released in the cell by recombination of hydrogen. The power of the dilution refrigerator considered is about 20 mW, therefore no problem should occur.

The power released in the cell by beam ionization losses (see Sec. 3.1) is about 40 $\mu$W, which is not a matter of concern.

Beam interactions with the gas include also Mott and Møller scattering. At very low momentum transfers this scattering is integrated into the ionization losses. Potentially, the higher energy recoil particles can be absorbed in the cell material and provide additional heating. We estimated the full power, transferred to protons in Mott scattering, making a cut off for the momentum transfer at 2 keV (the atom size), as $\sim 2 \cdot 10^{-8}$ W, which is negligible.

A problem may occur with a beam halo, or with a poor beam tune, when the beam is scraping on aperture elements upstream of the target. High energy electrons would make showers in the dilution refrigerator and a large fraction of their energy will be absorbed. The refrigerator may quench. This effect should be limited to ∼5 mW, which is about $10^7$ electrons at 3 GeV. In order to protect the target a shielding must be installed in front of it. A 1-inch diameter beam pipe should be surrounded by a lead shielding about 20 cm thick and broad enough to cover the sensitive cryogenic elements.

The heat load from thermal radiation in the beam pipe is very large. Therefore, a set of cold screens must isolate the cell from the rest of the beam pipe. The screens must have about 1 cm diameter holes for the beam.

# Chapter 4

# Application of the Atomic Target to Møller Polarimetry

This feasibility study is limited to the possible application of the target discussed to the existing Møller polarimeter in Hall A at JLab [7]. The results are, however, more generic and are largely applicable to other conditions.

## 4.1 Polarimeter Parameters

### 4.1.1 Polarimeter Acceptance

Hall A polarimeter selects electrons, scattered close to the horizontal plane, in angular ranges of about $75^\circ < \theta_{CM} < 105^\circ$ and $-5^\circ < \phi_{CM} < 5^\circ$, where $\theta_{CM}$ and $\phi_{CM}$ are the polar and azimuth angles of the scattered electrons in the center of mass frame. Coincidences of two secondary electrons are identified and counted. The acceptance of the polarimeter may be distorted by the strong magnetic field of the target trap. Monte Carlo simulation of the polarimeter optics shows that a 7 T solenoid in the target area would rotate the scattering plane by about 5°, and the polarimeter acceptance changes from $-5^\circ < \phi_{CM} < 5^\circ$ to about $0^\circ < \phi_{CM} < 10^\circ$. This makes no effect on the results. The polarimeter acceptance depends on the longitudinal coordinate of the interaction point. At the lowest beam energy the dependence is the strongest and the effective target length is about 10 cm. At higher energies the effective length is larger.

### 4.1.2 Target Density and Statistical Accuracy

The beam polarization at JLab is normally about 80%. The target of supermendur is 30 $\mu$m thick along the beam, containing about $6.7 \cdot 10^{21}$ electrons/cm$^2$. The target polarization is about 8%. At the regular beam current used for polarimetry of 0.3 $\mu$A the coincidence counting rate is about 50-200 kHz, depending on the beam energy. At the average rate of 100 kHz, a relative statistical accuracy of 1% can be achieved in about 2 min. A

hydrogen target 10 cm long[1] with a density of $3 \cdot 10^{15}$ electrons/cm$^3$ provides $3 \cdot 10^{16}$ electrons/cm$^2$. The maximum beam current allowed by the accelerator can be used with the hydrogen target. We assume here an easily available current of 30 $\mu$A, though currents up to 100 $\mu$A have been delivered . The time needed to achieve the same 1% accuracy would be 2 min$\times \frac{6.7 \cdot 10^{21} cm^{-2}}{3 \cdot 10^{16} cm^{-2}} \times 0.08^2 \times \frac{0.3 \mu A}{30 \mu A} \approx$ 30 min. This is an acceptable time, in particular if the measurements are done in parallel with the main experiment.

### 4.1.3 Filling and Cleaning Time

Preparations of the cell include ramping the magnetic field (less than 1 h), building the helium film (less than ∼5 min) and hydrogen filling (∼10 min - see Sec. 2.3). Cleaning the cell from hydrogen can be done in different ways, like by reducing the magnetic field, by forced recombination of hydrogen etc. The gas can be relatively quickly removed by enforcing hydrogen recombination on a special element inside the cell (see Sec. 2.3). This procedure has to be optimized, since the full energy released by recombination is ∼1 J. A large power released can cause all the helium film to evaporate. Therefore, the recombination should go gradually, perhaps at the edge of the cell, in a low density area.

### 4.1.4 Background

The no-target background was measured by the Hall A Møller polarimeter in situ, at room temperature, with the 4. GeV electron beam of 30 $\mu A$. The coincidence rate was about 1 Hz, corresponding to about 1% of the expected coincidence rate with the hydrogen target at this beam current. The single-arm rate was about 600 Hz. Although noticeable, this background can be easily measured on the regular basis by removal of the atomic hydrogen gas from the cell (see Sec. 4.1.3).

Another source of background is electron-nuclei scattering on the target material. The polarimeter aperture accepts particles with the energies from 30% to 70% of the beam energy. Since the electrons, "regularly"scattered at small angles, practically preserve their initial energy, only radiative scattering may provide a background for the polarimeter. Indeed, the observed "single arm" background in Hall A polarimeter, amounting to about 40-80% of the "double arm" coincidence rate, is well described by radiative elastic scattering off the target nuclei. Coincidence requirement reduces this background to a sub-percent level, though its exact measurement on this level is difficult. In case of the hydrogen target the initial "single arm" background is expected to be 5-10 times lower, which should limit a possible coincidence background to about 0.1%.

A way to measure the residual gas background, coming from helium and other residual gasses in the beam pipe, is to measure the counting rate before filling the cell with hydrogen. One can monitor the gas pressure throughout the polarization measurement using a long

[1] The effective target length depends on the beam energy, because of the polarimeter acceptance. At the lowest energy considered - 0.850 GeV, the effective length is about 10 cm, while at 5 GeV it is about 20 cm

pipe attached to the edge of the cell, where the hydrogen density is very low. This method has been used before (see Sec. 2.5.4).

An additional, and a very powerful way to measure the background continuously would be to equip the Møller polarimeter with microstrip detectors, located between the target and the first quadrupole magnet, in order to measure the trajectories of the scattered electrons and reconstruct the point of interaction origin. An accuracy of about 5 mm for the longitudinal coordinate of the origin point would be sufficient to limit the selected interactions to the central area of the target only, while the rate measured at the edges of the cell will provide the background.

### 4.1.5 Target Polarization Reversal

Target polarization reversal is useful for reduction of the beam current asymmetries, driven by the beam helicity, or other possible false asymmetries. These beam asymmetries at JLab are sometimes as high as 1%, but typically they are better than 0.1%. With the ferromagnetic targets the Møller asymmetry observed is about $\mathcal{P}_{beam} \cdot \mathcal{P}_{targ} \cdot A_M \sim 4\%$, where $\mathcal{P}$-s denote the beam and target polarizations and $A_M \approx 7/9$ is the analyzing power of the process. Evidently, a false asymmetry of 1%, coming from the beam would give a 25% relative error for the beam polarization measurements. The beam current monitors are used to correct for the beam asymmetry. Since these devices are not very linear at low currents used, the residual relative error for the beam polarization could be about 1%. Fortunately, averaging the results obtained with opposite target polarizations cancels out this false asymmetry. In practice, the target polarization of Hall A polarimeter is reversed every 2-5 min.

If the hydrogen target is used, the asymmetry observed would be about 50%. Therefore, the influence of the beam asymmetry would be a factor of 10 smaller than now. Furthermore, the hydrogen target would operate at beam currents of 30-100 $\mu$A. The beam current monitors are more precise in this range than at 0.3-1 $\mu$A used with the ferromagnetic targets. One may conclude that the frequent target polarization reversal is not needed for polarimetry with the hydrogen target.

If polarimetry is running in parallel with the main experiment, the hydrogen target may become the source of a sizable false asymmetry, in particular for parity violation experiments where the effect measured could be $\sim 10^{-6}$, or even smaller. To cancel out a possible false asymmetry one has to take data with opposite polarizations of the atomic hydrogen target. Inverting the target polarization, say, once per day should not pose a technical problem. It may happen at low beam energies that the target solenoid affects the beam focusing for the main experiment. In such a case it might be not useful to take data during the solenoid reversal. This would limit the reasonable frequency of the target reversals.

### 4.1.6 Effective Target Polarization

The effective target polarization, after subtracting the non-hydrogen background (see Sec. 4.1.4) is very close to 100%. The identified sources of depolarization are listed in Tab. 4.1.

| No | $\delta\mathcal{P}$ | | description | | Beam dependence | |
|---|---|---|---|---|---|---|
| | estimate | upper limit | source | Section | $\mathcal{I}_b$ | $f(\mathcal{I}_b)$ |
| 1 | 0.0005% | 0.001% | $\|a\rangle$ state $\|\uparrow\downarrow\rangle$ component | 2.1 | - | - |
| 2 | 0.001% | 0.002% | $H_2$ molecules | 2.5.1 | - | - |
| 3 | 0.0004% | 0.001% | $\|c\rangle$ and $\|d\rangle$ states | 2.5.2 | - | - |
| 4 | $10^{-11}$ | $10^{-11}$ | excited states | 2.5.3 | - | - |
| 5 | $10^{-11}$ | $10^{-10}$ | gas heating | 3.1 | 100 $\mu$A | $\propto \mathcal{I}_b$ |
| 6 | 0.0003% | 0.001% | free electrons / ions | 3.2 | 100 $\mu$A | $\propto \mathcal{I}_b$ |
| 7 | 0.002% | 0.005% | transitions by beam RF | 3.3.1 | 100 $\mu$A | $\propto \mathcal{I}_b^2$ |
| | 0.004% | 0.01% | total | | | |

Table 4.1: The identified sources of the target depolarization.

We would like to emphasize that the estimates for contributions 1-4 (not associated with the beam) are bases on the well studied properties of such storage cells. The parameter to control is the lifetime of polarized gas in the cell (with feeding turned off). This easily measurable parameter provides the rate of atoms recombinations and conversions. The contamination scales with this rate, and the relations are well understood.

The components 5-7, are associated with the beam. Again, the gas lifetime provides a critical parameter to understand the additional average conversion rate. Also, these effects can be studied by varying the beam current and other beam parameters.

The component 7 depends on the beam parameters as $\mathcal{I}_b^2/\mathcal{F}$. One may use a different CEBAF repetition rate (so called "G0 structure"). Keeping the same current one may use a rate of about 20 times lower than normal, increasing the depolarization effect #7 by a factor 20. But the most sensitive test would be tuning the magnetic field of the solenoid to overlap a peak in the gas spectral density distribution with a beam resonance, increasing the effect of depolarization by a factor of ∼100. This will help to put a limit on the depolarization at a 0.01% level.

The component 6 can be studied by varying the cleanup voltage. With voltage set to zero the effect is about $10^4$ higher. This will allow to put a limit on the depolarization at a 0.01% level.

The component 5 can be studied by measuring the dependence of the gas density in the beam area on the beam current, using the Møller scattering rate. The density is a known function of temperature, which defines the gas polarization.

The upper limit on the expected target depolarization is about 0.01%, which is well below the other experimental errors.

### 4.1.7 Polarimetry Systematic Error

Adding in quadrature the systematic errors, important for the present Hall A Møller polarimeter, gives the total systematic error of about 3%. Scaling these errors to the hydrogen target option leaves only those:

- Average analyzing power 0.3%;
- Background 0.1%.

At this level of accuracy, some other errors, neglected before, may become significant and more work has to be done to identify them. Still, a 0.5% error seems achievable and a 1% error certain.

## 4.2 Target Influence on the Beam

The possibility of the polarimeter operation in parallel with the experiment is very important. Several problems may, however, occur.

The beam optics, in particular at low energies, might be distorted by the solenoid field, which couples the X and Y projections of the trajectory. This may affect the beam focusing at the main target, 17 m downstream of the polarimeter target. The first evaluation by the JLab beam optician was favorable for energies larger than about 2 GeV, but more work is needed.

Another possible influence comes from interactions with the atomic hydrogen target. The target thickness of $3 \cdot 10^{16}$ electrons/cm$^2$ can be compared with the existing residual gas, which in a $\sim$50 m long beam pipe section gives a comparable amount of $\sim 2 \cdot 10^{16}$ electrons/cm$^2$. No considerable deterioration of the beam quality would be caused by the hydrogen target due to interactions. The influence of the multiple scattering in the polarimeter target on the beam spot on the main target can be compared with the influence made by the residual gas. A 10 m long section of the beam pipe filled with residual gas, about 40 m upstream of the main target, would give the same effect as the hydrogen target. Therefore, no significant change of the beam spot should happen because of the hydrogen target.

# Chapter 5

# Conclusion

The considerations above show that a stored, longitudinally electron-spin-polarized atomic hydrogen can be used as a pure, 100% polarized gas target. A thickness of at least $6 \cdot 10^{16}$ electrons/cm$^2$ can be reached with a target diameter of 4 cm and a length of 20 cm along the beam. Møller polarimeter, equipped with such a target would provide a superb systematic accuracy of about 0.5%. The polarized hydrogen gas should be stable in presence of a 100 $\mu$A CEBAF beam. Some care should be taken in tuning the magnetic field of the storage cell in order to avoid the resonant depolarization of the gas by the beam.

# Appendix A

# Auxiliary Calculations

## A.1 Beam-Induced Effects

### A.1.1 Parameters of the Beam and the Trap

#### Beam

The beam parameters considered are as follows:

- $\sigma_{Bt} = \tau = 0.5$ ps - bunch time width (RMS) in LAB frame
- $\sigma_{Br} = 100$ $\mu$m - bunch radial width (RMS) in LAB frame
- $\mathcal{F} = 499$ MHz - bunch repetition rate
- $\gamma \sim 10^4$ - beam $\gamma$-factor
- $\mathcal{I}_b = 100$ $\mu$A - the highest beam beam current used with polarized beams

Gaussian shapes are assumed for both the longitudinal and transverse beam profiles.

#### Hydrogen Trap

The atomic hydrogen trap consists of a copper pipe being a part of the dilution refrigerator, kept at 300 mK.
The parameters of the copper pipe are:

- $L = 0.4$ m - pipe length
- $r_0 = 0.02$ m - pipe diameter
- $\sigma = 10^{11}$ (ohm·m)$^{-1}$ - copper conductance at 300 mK
- $C_{Cu} = 1.5 \cdot 10^{-3}$ J $\cdot$ kg$^{-1}$ $\cdot$ K$^{-1}$ - copper specific heat at 300 mK
- $\rho_{Cu} = 8960$ kg $\cdot$ m$^{-3}$ - copper density
- $T \sim 0.3$ K - the temperature
- $\frac{dN}{dV} \sim 3 \cdot 10^{15}$ atoms/cm$^2$ - the gas density

**Other Parameters and Constants Used**

Some derived parameters are used:

- $q = \mathcal{I}_b/\mathcal{F} = 0.2$ $p$C - bunch charge
- $\sigma_{Bz} = \sigma_{Bt} \cdot c = 150\mu$m - bunch longitudinal width (RMS) in LAB frame
- $\rho(z,r) = q/(\sqrt{2\pi}\sigma_{Bz}) \cdot exp(-z^2/(2\sigma_{Bz}^2)) \times (1/(2\pi\sigma_{Br}^2) \cdot exp(-r^2/(2\sigma_{Br}^2))$ - charge density of a bunch (LAB)
- $\omega_b = 2\pi/\sigma_{Bt} = 1.3 \cdot 10^{13}$ s$^{-1}$ - typical frequency associated with the bunch length. We will show later that this is indeed the characteristic frequency of the process.
- $\omega_\circ = 2\pi \cdot \mathcal{F}$ - bunch repetition frequency
- $T = \mathcal{F}^{-1}$ - repetition period

The values of used constants:

- $\varepsilon_\circ = 8.854 \cdot 10^{-12}$ F/m
- $\mu_\circ = 4\pi \cdot 10^{-7}$ N/A$^2$
- $k = 8.6173 \cdot 10^{-5}$ eV/K - Boltzmann constant

### A.1.2 Calculation of the Electromagnetic Field

The bunch creates an electromagnetic pulse in the pipe. The fields are calculated in two steps: at first, the electric field created by the bunch charge is calculated in the rest frame of the bunch, then the field is boosted to the Lab frame. The variables in the bunch rest frame are marked with prime sign. In this frame, only the radial component of the field matters.

Let us assume that the bunch moves along the z axis in the Lab frame and crosses $z = 0$ at $t = 0$. The bunch rest frame has the same orientation as the Lab frame and its center is at the center of the bunch. We are mostly interested in the field close to the beam, the accuracy at the peripheral area of the pipe is not very important. The bunch size (RMS) in the bunch rest frame is $\gamma$ times larger than in the Lab frame, namely 25-150 cm at beam energies of 0.85-5.0 GeV, which is much larger than the cell radius of 2 cm. In the limit $r \ll \sigma_{Bz}\gamma$ the flux through a cylinder of the radius $r$ is:

$$\varepsilon_\circ E_r^{'}(z^{'},r) \cdot 2\pi r = \int_0^r d\xi \cdot 2\pi\xi \cdot \rho^{'}(z^{'},\xi) = \rho^{'}(z^{'}) \cdot (1 - exp(-\frac{r^2}{2\sigma_{Br}^2})) \tag{A.1}$$

where

$$\rho^{'}(z^{'}) = \frac{q}{\sqrt{2\pi}\sigma_{Bz}\gamma} \cdot e^{-\frac{z^{'2}}{2(\sigma_{Bz}\gamma)^2}} \tag{A.2}$$

is the longitudinal charge density along the bunch. The radial component of the electric field is:

$$E_r^{'}(z^{'},r) = \frac{q}{2\pi\varepsilon_\circ}\frac{1}{\sqrt{2\pi}\sigma_{Bz}\gamma} \cdot exp(-\frac{z^{'2}}{2(\sigma_{Bz}\gamma)^2})(1 - exp(-\frac{r^2}{2\sigma_{Br}^2}))\frac{1}{r} \tag{A.3}$$

Now, let us boost the field into the Lab frame using the Lorentz formula:

$$E_r(z,t) = \gamma(E_r^{'}(z^{'}) - \vec{V} \times \vec{B}^{'}(z^{'})) \tag{A.4}$$

$$B_r(z,t) = \gamma(B_r^{'}(z^{'}) + \vec{V} \times \vec{E}^{'}(z^{'})/c^2) \tag{A.5}$$

$$z^{'} = \gamma(z - V \cdot t) \tag{A.6}$$

where $\vec{V} \sim (0,0,c)$ is the bunch velocity (along z in our case).

We calculate the radial electric field and the tangential (along $\phi$) magnetic field. Indeed, $\vec{V} \times \vec{E}^{'}(z^{'},r) = V \cdot E'_r$ is directed along $\vec{d\phi}$. Using $c^{-2} = \varepsilon_\circ \mu_\circ$ we obtain:

$$E_r(z,r,t) = \frac{q\gamma}{2\pi\varepsilon_\circ} \frac{1}{\sqrt{2\pi}\sigma_{Bz}\gamma} \cdot exp(-\frac{(z-Vt)^2\gamma^2}{2(\sigma_{Bz}\gamma)^2})(1 - exp(-\frac{r^2}{2\sigma_{Br}^2}))\frac{1}{r} =$$

$$= \frac{q\mu_\circ c}{2\pi\sqrt{2\pi}\tau} \cdot exp(-\frac{(z/c-t)^2}{2\tau^2})(1 - exp(-\frac{r^2}{2\sigma_{Br}^2}))\frac{1}{r} \tag{A.7}$$

The field profile repeats the bunch profile. The field is $\gamma$ times larger than in the rest frame and is located in a thin disk around the bunch. In order to see the dependence of the result on the input parameters more clearly let us define a dimensionless function:

$$G(r) = (1 - exp(-\frac{r^2}{2\sigma_{Br}^2}))\frac{r_\circ}{r}; \qquad G(r_\circ) = 1 \tag{A.8}$$

where $r_\circ$ is the pipe radius. In the same way

$$B_T(z,r,t) = \frac{q\mu_\circ}{2\pi\sqrt{2\pi}\tau r_\circ} \cdot exp(-\frac{(z/c-t)^2}{2\tau^2}) \cdot G(r) = E_r(z,r,t)/c \tag{A.9}$$

For the conditions used the fields in the pulse reach their maximum at $r = 160$ $\mu$m, namely $E_r(0,r,0) = 4.31 \cdot 10^4$ V/m and $B_r(0,r,0) = 1.44 \cdot 10^{-4}$ T, while at r=2 cm the fields are 478 V/m and $1.59 \cdot 10^{-6}$ T (see Fig. A.1).

Let us re-write Eq. A.9:

$$B_T(z,r,t) = B_T(r) \cdot exp(-\frac{(z/c-t)^2}{2\tau^2}) \tag{A.10}$$

The energy of the field flows along the beam $\mathcal{S} = Re(EH^*)/2 = |B|^2 c/\mu_\circ/2$ The density of the energy flux of the electromagnetic field of a bunch, passing through the pipe cross section is:

$$\frac{dw(r)}{dS} = \frac{c}{2\mu_\circ} B_T(r)^2 \cdot \int_{-\infty}^{\infty} dt\ exp(-\frac{2t^2}{2\tau^2}) = \frac{1}{2\mu_\circ} B_T(r)^2 \cdot \sqrt{\pi}c\tau =$$

$$\frac{\mu_\circ c}{4\sqrt{\pi}\tau} \left(\frac{q}{2\pi r_\circ}\right)^2 \cdot G(r)^2 \tag{A.11}$$

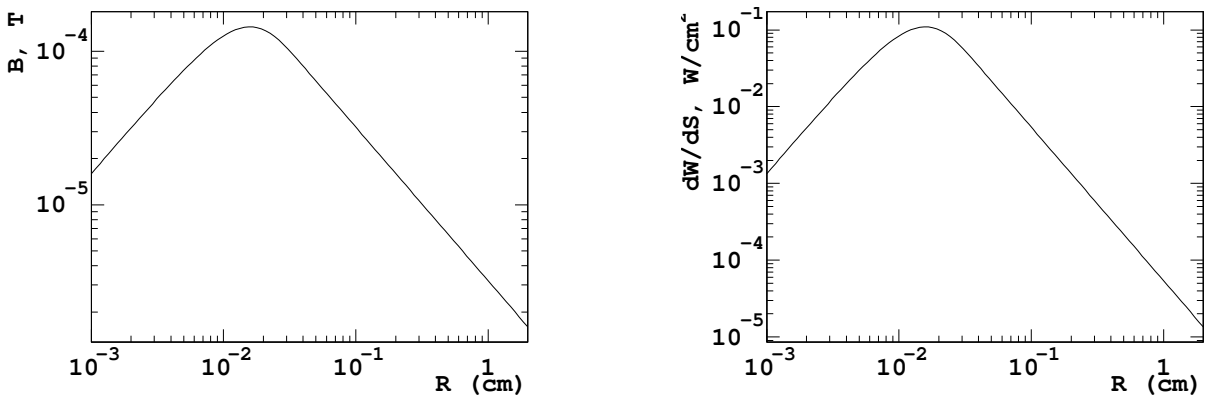


Figure A.1: Left: Tangential magnetic field of the 100 $\mu$A CEBAF beam at the pulse maximum. Right: The density of the energy flux of the beam electromagnetic field.

The radial dependence of the flux is show on Fig. A.1. In order to integrate the power flux over the pipe cross section let us make an approximation for $R > 5\sigma_{Br}$:

$$\frac{1}{r_\circ^2}\int_0^R dr\cdot 2\pi r\cdot G(r)^2 = \int_0^R dr\cdot 2\pi r\frac{(1-e^{-\frac{r^2}{2\sigma_{Br}^2}})^2}{r^2} = 2\pi\int_0^{R/\sigma_{Br}} d\xi\frac{(1-exp(-\xi^2/2))^2}{\xi}$$
$$\approx 2\pi\cdot(1.205+\ln\frac{R}{5\sigma_{Br}}) \qquad (A.12)$$

The full power of radiation coming down the pipe is determined using the repetition rate $\mathcal{F}$:

$$W=\mathcal{F}\int_0^{r_\circ} dr\cdot 2\pi r\cdot\frac{w(r)}{dS}\approx\frac{\mu_\circ c\mathcal{I}_b^2}{8\pi\sqrt{\pi}\tau\mathcal{F}}(1.205+\ln\frac{r_\circ}{5\sigma_{Br}})\approx 2\ mW \qquad (A.13)$$

### A.1.3 Electromagnetic Radiation from Beam Pipe Irregularities

Additionally to the radiation coming with each beam bunch there is a radiation, detached from beam, generated on beam pipe irregularities, like pipe diameter changes. The beam loses energy due to this radiation, in contrast with the radiation described in Sec. A.1.2. The radiation is minimized if the beam pipe has the same diameter everywhere. In our case, beyond the ends of the cell pipe there must be a break to a larger vacuum chamber in order to provide the thermal insulation needed. This break acts like a cavity. Let us approximate this cavity with a regular cavity used in the beam lines at CEBAF. A typical voltage generated on this cavity by the beam bunch of a given charge is $\eta\sim$10 V/pc. From this, we can estimate the full power lost by the beam to radiation:

$$W_c=\eta\cdot\mathcal{I}_b^2/\mathcal{F}\approx 0.2\ mW \qquad (A.14)$$

Only a small fraction of this radiation enters the downstream beam pipe, most of it would escape the beam area transversally, since the vacuum chamber is wide in this area.

Therefore, inside the trap pipe, the radiation from pipe irregularities is at least 10-100 times weaker than the radiation created by the passing beam and we neglect it.

### A.1.4 Spectral Density of the Electromagnetic Field

In order to estimate the impact of the electromagnetic radiation we have to calculate its spectral density. At a given point ($z = 0$ for example) the field has a form of Eq. A.10:

$$f(t) = f_\circ \cdot exp(-\frac{t^2}{2\tau^2}), \tag{A.15}$$

where $f_\circ$ is a function of the radius $r$. Here we use a shorter symbol $\tau$ for the RMS of the bunch duration $\tau = \sigma_{Bt}$. First, let us calculate the Fourier transform of one single bunch:

$$f(t) = \frac{1}{\sqrt{2\pi}} \int_{-\infty}^{\infty} d\omega \cdot \hat{f}(\omega) e^{i\omega t}, \tag{A.16}$$

where

$$\hat{f}(\omega) = \frac{1}{\sqrt{2\pi}} \int_{-\infty}^{\infty} dt \cdot f(t) e^{-i\omega t} = f_\circ \cdot \tau \cdot exp(-\frac{\omega^2\tau^2}{2}) \tag{A.17}$$

The spectrum starts dropping at frequencies $\nu = \frac{\omega}{2\pi} \sim \frac{1}{\tau} = 320$ GHz.

The bunches arrive with a period $T$. The appropriate Fourier series is:

$$f(t) = \sum_{k=-\infty}^{\infty} \hat{f}_k \cdot e^{i\omega_\circ k t}, \tag{A.18}$$

where $\omega_\circ = 2\pi/T$ and

$$\begin{aligned} \hat{f}_k &= \frac{1}{T} \int_{-T/2}^{T/2} dt \cdot f(t) e^{-i\omega t} \approx \frac{1}{T} \int_{-\infty}^{\infty} dt \cdot f(t) e^{-i\omega t} = f_\circ \sqrt{2\pi} \cdot \frac{\tau}{T} \cdot exp(-\frac{\omega_\circ^2 k^2 \tau^2}{2}) \\ &= f_\circ \frac{\tau\omega_\circ}{\sqrt{2\pi}} \cdot exp(-\frac{\omega_\circ^2 k^2 \tau^2}{2}). \end{aligned} \tag{A.19}$$

The integral can be taken in the infinite limits since the width of the bunch is much smaller than the period: $\tau \ll T$.

The Fourier series for the magnetic field at $z = 0$ is (see Eq. A.9 and Eq. A.8):

$$\hat{B}_k(r) = \frac{\tau\omega_\circ}{\sqrt{2\pi}} \cdot exp(-\frac{\omega_\circ^2 k^2 \tau^2}{2}) \frac{q\mu_\circ}{2\pi\sqrt{2\pi}\tau} \cdot G(r) = \frac{\mu_\circ \mathcal{I}_b}{2\pi r_\circ} \cdot exp(-\frac{\omega_\circ^2 k^2 \tau^2}{2}) \cdot G(r) \tag{A.20}$$

### A.1.5 Eddy Currents

A bunch moving inside of the conductive pipe induces an electric charge image on the pipe, which moves along the pipe with the bunch, creating "eddy currents". These currents flow in a thin "skin" of the pipe, the skin depth depends on the characteristic frequency of the electromagnetic pulse. The length of the electromagnetic pulse, created by a point-like moving charge at a distance $r = 0.02$ m from the beam axis is about $r/\gamma \sim 2\ \mu$m $\ll \sigma_{Bz} = 150\ \mu$m - the bunch length. Therefore the pulse shape repeats the bunch shape and we may use $\omega_b$ for the characteristic frequency.

#### Skin Depth and Power Absorption

The skin depth $\delta$ estimate is crucial for the power loss calculation. The effect depends, along with already defined frequency $\omega$ and conductance $\sigma$, on several important parameters:

- $\tau_c$ - mean collision time of electrons in the material
- $\ell$ - mean free path of electrons in the material
- $\omega_p = \sqrt{\frac{N \cdot q_e^2}{\varepsilon_0 m_e}} \approx 1.6 \cdot 10^{16}$ s$^{-1}$ - the plasma frequency, where $N$ is the electron density and $q_e$ ,$m_e$ are the electron charge and mass.

At frequencies $\omega \ll \omega_p$ three different physics regimes occur, depending on the relative values of these parameters:

(1) Normal skin effect - low frequency regime: $\omega\tau_c \ll 1$ and $\ell \ll \delta$. The smallest spacial parameter is the mean free path $\ell$. So, on the length of the mean free path the field does not change much. In this case a local (the same space and time) relation $\vec{j} = \sigma\vec{E}$ is valid.

(2) Anomalous skin effect - a thin skin depth: $\delta \ll \ell$ and $\delta \ll \ell/\omega\tau_c$, while there is no limit for $\omega\tau_c$. The lowest spacial parameter is $\delta$.

(3) High frequency, or infrared limit - $\omega\tau_c \gg 1$ and $\ell/(\omega\tau_c) \ll \delta$. In normal metals at normal temperatures this condition is fulfilled in the infrared range.

In order to calculate the power loss let us consider the Maxwell equations for conductors in empty space, neglecting the term $\frac{\partial\vec{D}}{\partial t}$:

$$rot\vec{H} = \vec{j}; \quad rot\ \vec{E} = -\frac{\partial\vec{B}}{\partial t} \tag{A.21}$$

$$div\vec{B} = 0; \quad div\vec{D} = 0 \tag{A.22}$$

Assuming no magnetic materials: $\vec{B} = \mu_\circ\vec{H}$. Let us consider the simplest low frequency regime (1), which adds an equation:

$$\vec{j} = \sigma\vec{E} \tag{A.23}$$

Then:

$$\Delta\vec{H} = \mu_\circ\sigma\frac{\partial\vec{H}}{\partial t} \tag{A.24}$$

Assuming a time dependence as $e^{-i\omega t}$ we obtain:

$$\Delta\vec{H} = -i\mu_\circ\sigma\omega\vec{H} \tag{A.25}$$

Let us consider high enough frequencies, that the skin depth is much smaller than the conductor size. On the boundary with metal the tangential components of $\vec{H}$ and $\vec{E}$ are conserved. Let us assume that metal occupies all space at $z > 0$. $\vec{H}$ depends only on time and $z$. Since $div\vec{H} = 0$ and the field somewhere inside the metal is zero, $H_z = 0$ everywhere. We can rewrite Eq. A.25 as:

$$\frac{\partial^2\vec{H}}{\partial^2 z} + k^2\vec{H} = 0, \tag{A.26}$$

where

$$k = \sqrt{\sigma\mu_\circ\omega/2}(1+i) \tag{A.27}$$

Then, considering a solution as $\vec{H}_0 exp(ikz)$ we obtain

$$\vec{H} = \vec{H}_0 exp(-z/\delta)exp(iz/\delta - \omega t) \tag{A.28}$$

where

$$\delta = \sqrt{\frac{2}{\sigma\omega\mu_\circ}} = \sqrt{\frac{2\varepsilon_\circ c^2}{\sigma\omega}} \tag{A.29}$$

is the skin depth in the "low frequency" approximation (1). The electrical field is calculated using Eq. A.23

$$\vec{E} = \zeta\vec{H}\times\vec{n}, \tag{A.30}$$

where $\vec{n}$ is a vector normal to the surface and $\zeta$ is called impedance:

$$\zeta = \sqrt{\frac{\omega\mu_\circ}{2\sigma}}(1-i) = \sqrt{\frac{2\varepsilon_\circ c^2}{\sigma\omega}}(1-i) \tag{A.31}$$

Both the $\vec{H}$ and $\vec{E}$ are tangential on the surface and are the same inside and outside of the conductor. The power flux into the conductor is described by Poynting vector averaged over time:

$$\mathcal{S} = Re(\vec{E}\vec{H}^*)/2 = Re(\zeta\,|H|\,|H|^*)/2 = Re(\zeta)\,|H|^2/2 = \sqrt{\frac{\omega\mu_\circ}{2\sigma}}\,|H|^2/2 = \omega\delta\mu_\circ\,|H|^2/4 \tag{A.32}$$

If we apply the "low frequency" limit to our case we obtain:

$$\delta_{lf} = \sqrt{\frac{2\varepsilon_\circ c^2}{\sigma\omega}} = 1.1\cdot 10^{-9}\ m \tag{A.33}$$

Now, let us return to our case. Our characteristic frequency is $\omega_b \ll \omega_p$. The other parameters for copper at 0.3 K were estimated using the known conductance, density and

assuming that there is one free electron per atom. This estimate is valid, in fact, in the low frequency limit. We assume that all the electrons are drifting in electrical field with a velocity $v_d = q_e E/m_e \cdot \tau_c$, depending on the time between collisions $\tau_c$. The current in the conductor is $j = N q_e v_d$. On the other hand, the current can be expressed using the conductance: $j = \sigma E$, and

$$\tau_c = \frac{\sigma m_e}{N q_e^2} \approx 4.2 \cdot 10^{-11}\ s \tag{A.34}$$

We see that $\omega_\circ \tau_c \approx 550 \gg 1$. Therefore the low frequency approximation (1) is not applicable in our case. In order to estimate the mean free path $\ell$ in this framework we have to know the electric field in the metal. Let us make an upper limit estimate. We will see later that in our case the maximum magnetic field parallel to the metal surface is about $B = 2 \cdot 10^{-6}$ T. In the low frequency approximation the associated electric field inside the metal is $B \cdot c\sqrt{2\varepsilon\omega/\sigma} \approx 0.03$ V/m. Therefore $v_d \approx 20$ m/s and

$$\ell \approx v_d \cdot \tau_c \sim 10^{-9}\ m \tag{A.35}$$

Therefore $\ell/(\omega\tau_c) \sim 10^{-12}$ m seems much smaller than a reasonable skin depth $\delta$ and we can use the "infrared" approximation (3) of the skin effect. Indeed, we will prove that $\delta \gg \ell/(\omega\tau_c)$.

A solution for the "infrared" approximation [30] gives

$$\delta = c/\omega_p = 1.8 \cdot 10^{-8}\ m, \tag{A.36}$$

not dependent on the frequency. It is about 20 times larger than the "low frequency" estimate of Eq. A.33. The field inside the metal drops exponentially.

It is pointed out in [30] that Eq. A.36 is obtained neglecting the electron collisions and therefore no absorption of electromagnetic waves in the metal happens. Indeed, the impedance obtained is purely imaginary:

$$\zeta = -i\omega\delta\mu_\circ \tag{A.37}$$

while the energy absorption is defined by real the part of $\zeta$.

Since it is not clear how good is the assumption for no electron collisions we will try to estimate the losses in a different phenomenological approach. The skin depth can be evaluated using the generalized refractive index of the metal:

$$n = n_R - i \cdot n_I, \tag{A.38}$$

where $n_R$ and $n_I$ are positive and the latter is responsible for the the wave attenuation. The wave inside the metal is suppressed by a factor $exp(-\omega z \cdot n_I/c)$ and the skin depth is:

$$\delta = \frac{c}{\omega n_I} \tag{A.39}$$

There is a general description of the refractive index using a simple model for electron motion in material [32]:

$$n^2 = 1 + \frac{\sigma}{i\varepsilon_\circ\omega(1 + i\omega\tau_c)}, \tag{A.40}$$

where $\sigma$ is the conductance and $\tau_c$ is the mean time between collisions for the electrons in metal. It is evaluated as:

$$\tau_c \approx \frac{m \cdot \sigma}{N \cdot q_e}, \tag{A.41}$$

At low frequencies, such as $\omega\tau_c \ll 1$, an approximation is valid: $n^2 \approx -i\sigma/(\varepsilon_\circ\omega)$, and

$$n = \sqrt{\frac{\sigma}{2\varepsilon_\circ\omega}}(1-i) \tag{A.42}$$

The wave inside the material is suppressed by a factor $exp(-\omega z \cdot n_I/c)$ and the skin depth is:

$$\delta = \frac{c}{\omega n_I} = \sqrt{\frac{2\varepsilon_\circ c^2}{\sigma\omega}} \tag{A.43}$$

the same as in Eq. A.33. We calculated the refractive index in the range of

$$2.5 \cdot 10^{10}\ s^{-1} \ll \omega \ll 2 \cdot 10^{16}\ s^{-1} \tag{A.44}$$

or

$$7.5\ cm \gg \lambda \gg 100\ nm,$$

relevant for our case.

$$n^2 = -\frac{\sigma}{\varepsilon_\circ\omega_b^2\tau_c}(1 - i \cdot \frac{1}{\omega_b\tau_c}) = A \cdot e^{i\phi_0}, \tag{A.45}$$

where $A \approx \frac{\sigma}{\varepsilon_\circ\omega_b^2\tau_c}$ and $\phi_0 \approx \pi + \epsilon + 2\pi m$. In order to keep $n_R > 0$ and $n_I > 0$ we select $m = 1$. So,

$$n = \sqrt{A}e^{i(\frac{3}{2}\pi+\epsilon/2)} \approx \sqrt{\frac{\sigma}{\varepsilon_\circ\omega_b^2\tau_c}}(\frac{1}{2\omega_b\tau_c} - i) \approx 3 - 1500i, \tag{A.46}$$

the refractive index is nearly purely imaginary and the skin depth

$$\delta = \sqrt{\frac{\varepsilon_\circ\tau_c c^2}{\sigma}} \approx 1.8 \cdot 10^{-8}\ m, \tag{A.47}$$

does not depend on the frequency and matches very well the result in Eq. A.36!

In order to estimate the absorption let us use the general wave reflection/refraction formalism. In case of a plane wave propagating in a medium with the refractive index $n = n_1$ normally to a plane boundary of another medium with $n = n_2$ the relative reflected intensity can be expressed as:

$$\frac{I_{refl}}{I_0} = \frac{|n_1 - n_2|^2}{|n_1 + n_2|^2} \tag{A.48}$$

Assuming that the first medium is vacuum and using Eq. A.38 for the second one:

$$\frac{I_{refl}}{I_0} = \frac{|(1-n_R) + i \cdot n_I|^2}{|(1+n_R) - i \cdot n_I|^2} = \frac{(1-n_R)^2 + n_I^2}{(1+n_R)^2 + n_I^2} \tag{A.49}$$

Using Eq. A.46 we see that about $5 \cdot 10^{-6}$ of the incident power is not reflected but, presumably, absorbed. For an ideal metal ($\sigma \to \infty$) $n$ is purely imaginary and 100% of the wave is reflected. In "low frequency" limit about $1 \cdot 10^{-4}$ is not reflected, to be compared with $0.25 \cdot 10^{-4}$ obtained using Eq. A.32.

### Wave Absorption and Average Heating

Let us assume that the "low frequency" formula Eq. A.32 is applicable for the energy absorbed in the pipe, but let us use the skin depth as a parameter:

$$\mathcal{S} = \frac{\omega\delta}{4\mu_\circ}|B|^2 \tag{A.50}$$

The power release in the pipe is calculated in the same way as Eq. A.11, using $\omega = \omega_b = 2\pi/\sigma_{Bt}$

$$P = \mathcal{F}\cdot 2\pi r_0 L\cdot\int_{-\infty}^{\infty} dt\ \mathcal{S} = \delta\frac{\mathcal{I}_b^2\mu_\circ\cdot L}{\mathcal{F}\cdot 8\sqrt{\pi}\tau^2 r_0} \tag{A.51}$$

For estimating the upper limit on the power let us use the larger skin depth we obtained in Eq. A.36 $\delta = 1.8\cdot 10^{-8}\ m$:

$$P \approx 3\cdot 10^{-6} W \tag{A.52}$$

We should keep in mind that in this approximation the impedance is nearly purely imaginary and the power absorption should be much lower than described by Eq. A.50. Therefore we can say that in fact

$$P < 3\cdot 10^{-6} W \tag{A.53}$$

This value can be compared with the known power release in such cells during normal operations. With the typical hydrogen atoms recombinations rate of $10^{15}$ s$^{-1}$ (see Sec. 2.3) the power release is the cell is ∼1 mW. The CEBAF beam average influence is negligible.

### Heating by a Beam Pulse

The beam pulse releases some finite power into the cell. Due to a very small heat capacity of copper at 0.3 K, the temperature rise during the pulse might not be negligible. Here we estimate this effect. Let us calculate the temperature rise of a copper ring of the radius $r_\circ$, length $\Delta z$ and thickness $\delta$, cause by one beam pulse:

$$\Delta T = \frac{2\pi r_0\Delta z}{2\pi r_0\Delta z\delta\cdot\rho_{Cu}\cdot C_{Cu}}\cdot\int_{-\infty}^{\infty} dt\ \mathcal{S} = \frac{\mathcal{I}_b^2\mu_\circ}{\mathcal{F}^2\cdot 16\pi\sqrt{\pi}\tau^2 r_0^2\cdot\rho_{Cu}\cdot C_{Cu}} \approx 2\cdot 10^{-7}\ \text{K} \tag{A.54}$$

The effect is negligible.

# Bibliography


[1] E. Chudakov and V. Luppov, "Møller polarimetry with atomic hydrogen targets," IEEE Trans. Nucl. Sci. **51**, 1533 (2004). 1

[2] P. S. Cooper *et al.*, Phys. Rev. Lett. **34**, 1589 (1975). 3

[3] B. Wagner, H. G. Andresen, K. H. Steffens, W. Hartmann, W. Heil and E. Reichert, Nucl. Instrum. Meth. **A294** (1990) 541. 3

[4] J. Arrington *et al.*, Nucl. Instrum. Meth. **A311** (1992) 39. 3

[5] K. B. Beard *et al.*, Nucl. Instrum. Meth. **A361** (1995) 46. 3

[6] H. R. Band, G. Mitchell, R. Prepost and T. Wright, Nucl. Instrum. Meth. **A400**, 24 (1997). 3

[7] A. V. Glamazdin *et al.*, FizikaB **8**, 91 (1999) [arXiv:hep-ex/9912063]. 3, 27

[8] M. Hauger *et al.*, Nucl. Instrum. Meth. A **462**, 382 (2001) [arXiv:nucl-ex/9910013]. 3

[9] L. G. Levchuk, Nucl. Instrum. Meth. A **345**, 496 (1994). 3

[10] I. F. Silvera and J.T.M. Walraven, *in Progress in Low Temperature Physics, (Elsevier Science Publisher B.V., Amsterdam), Vol. X, 139-370 (1986).* 4, 7, 11

[11] I. F. Silvera, "Ultimate fate of a gas of atomic hydrogen in a liquid-helium chamber: Recombination and burial", Phys. Rev. **B29**, 3899 (1984). 6, 13

[12] I. F. Silvera and J.T.M. Walraven, Phys. Rev. Lett. **44**, 164 (1980). 7

[13] T. O. Niinikoski, in *C80-09-25.24* CERN-EP-80-227 *Presented at 1980 Int. Symp. on High Energy Physics with Polarized Beams and Polarized Targets, Lausanne, Switzerland, Sep 25 - Oct 1, 1980* 7

[14] D. Kleppner and T. J. Greytak, *In *Brookhaven 1982, Proceedings, High Energy Spin Physics-1982*, 546-565.*
D. Kleppner, *in Proceedings of the Workshop on Polarized Proton Ion Sources, Ann Arbor, 1981 (AIP Conference Proceedings, No. 80, 111 (1982)).* 7

[15] M. Mertig, A. V. Levkovich, V. G. Luppov and Y. K. Pilipenko, *In *Bonn 1990, Proceedings, High energy spin physics, vol. 2* 164-167.* 7

[16] M. Mertig, V. G. Luppov, T. Roser and B. Vuaridel, Rev. Sci. Instrum. **62**, 251 (1991). 8

[17] L. D. Landau, E. M. Livshitz, "Statistical Physics", Theoretical Physics, **vol X** Nauka, Moscow, 1979 8

[18] M. E. Gersh and R. B. Bernstein, "Calculated total elastic scattering cross sections for H(IS) at collision energies below 1 eV", Chem. Phys. Lett. **4**, 221 (1969). 9

[19] A. C. Allison and F. J. Smith, "Transport properties of atomic hydrogen", Atomic Data **3**, 317 (1971). 9, 22

[20] M. D. Miller and L. H. Nosanow, "Possible new quantum systems. II. Properties of the isotopes of spin-aligned hydrogen", Phys. Rev. **B15**, 4376 (1977). 9, 13, 17

[21] D. G. Friend and R. D. Etters, "A dilute hard-sphere Bose-gas model calculation of low-density atomic hydrogen gas properties", J. Low Temp. Phys. **39**, 409 (1980). 9, 22

[22] C. Lhuillier, "Transport properties in a spin polarized gas. III", Journal de Physique **44**, 1 (1983) 9

[23] W. Kolos, L. Wolniewicz, "Variational Calculation Of The Long-Range Interaction Between Two Ground-State Hydrogen Atoms", Chem. Phys. Lett. **24**, 457 (1974). 9

[24] G. H. van Yperen, I. F. Silvera, J.T.M. Walraven, J. Berkout, J. G. Brisson, "Direct Microscopic Study of Doubly Polarized Atomic Hydrogen by Electron-Spin Resonance", Phys. Rev. Lett. **50**, 53 (1983). 12

[25] W.A. Kaufman, T. Roser and B. Vuaridel, Nucl. Instrum. Meth. A **335**, 17 (1993). 14, 20

[26] K. Hagiwara *et al.* [Particle Data Group Collaboration], Phys. Rev. D **66**, 010001 (2002). 16

[27] A.P.M. Matthey, J.T.M. Walraven, and I.F. Silvera, Phys. Rev. Lett. **46**, 668 (1981).

[28] D.A. Bell *et al.*, Phys. Rev. B **34**, 7670 (1986). 14

[29] M. Knudsen, "Kinetic Theory of Gases", London: Methuen, 1952, pp.33-34. 15, 17

[30] E. M. Livshitz, L. P. Pitaevski, "Physical Kinetics", Theoretical Physics, **vol X** Nauka, Moscow, 1979 40

[31] AMI: American Magnetics, Inc., http://www.americanmagnetics.com/ 8, 21, 23

[32] R. P. Feynman, R. B. Leighton, M. L. Sands, "The Feynman Lectures on Physics," **vol 7**, London, UK : Addison-Wesley/Benjamin, 1964 40